

OPEN

Seasonal to Inter-Annual Variability of Primary Production in Chesapeake Bay: Prospects to Reverse Eutrophication and Change Trophic Classification

Lawrence W. Harding Jr.^{1*}, Michael E. Mallonee², Elgin S. Perry³, W. David Miller⁴, Jason E. Adolf⁵, Charles L. Gallegos⁶ & Hans W. Paerl⁷

Estuarine-coastal ecosystems are rich areas of the global ocean with elevated rates of organic matter production supporting major fisheries. Net and gross primary production (NPP, GPP) are essential properties of these ecosystems, characterized by high spatial, seasonal, and inter-annual variability associated with climatic effects on hydrology. Over 20 years ago, Nixon defined the trophic classification of marine ecosystems based on annual phytoplankton primary production (APPP), with categories ranging from “oligotrophic” to “hypertrophic”. Source data consisting of shipboard measurements of NPP and GPP from 1982 to 2004 for Chesapeake Bay in the mid-Atlantic region of the United States supported estimates of APPP from 300 to 500 g C m⁻² yr⁻¹, corresponding to “eutrophic” to “hypertrophic” categories. Here, we developed generalized additive models (GAM) to interpolate the limited spatio-temporal resolution of source data. Principal goals were: (1) to develop predictive models of NPP and GPP calibrated to source data (1982 to 2004); (2) to apply the models to historical (1960s, 1970s) and monitoring (1985 to 2015) data with adjustments for nutrient loadings and climatic effects; (3) to estimate APPP from model predictions of NPP; (4) to test effects of simulated reductions of phytoplankton biomass or nutrient loadings on trophic classification based on APPP. Simulated 40% decreases of euphotic-layer *chl-a* or TN and NO₂ + NO₃ loadings led to decreasing APPP sufficient to change trophic classification from “eutrophic” to “mesotrophic” for oligohaline (OH) and polyhaline (PH) salinity zones, and from “hypertrophic” to “eutrophic” for the mesohaline (MH) salinity zone of the bay. These findings show that improved water quality is attainable with sustained reversal of nutrient over-enrichment sufficient to decrease phytoplankton biomass and APPP.

Annual phytoplankton primary production (APPP) accounts for ~50 petagrams (=50 × 10¹² kg) of net primary production (NPP) in the oceans each year, half the global total for oceanic and terrestrial ecosystems according to a comprehensive review by Chavez *et al.*¹. Among ocean provinces, estuarine-coastal ecosystems have been characterized as biogeochemical “hot spots” by Cloern *et al.*² based on high contributions to APPP. In 1995, Nixon³ classified marine ecosystems as “oligotrophic” to “hypertrophic” based on APPP, with several estuaries in the mid-Atlantic region of the United States ranking toward the high end of the range (Fig. 1). Important advances

¹Department of Atmospheric and Oceanic Sciences, University of California, Los Angeles, Los Angeles, California, 90095, United States. ²Interstate Commission on the Potomac River Basin, United States Environmental Protection Agency, Chesapeake Bay Program Office, 410 Severn Avenue, Annapolis, Maryland, 21403, United States. ³Statistics Consultant, 377 Resolutions Rd., Colonial Beach, Virginia, 22443, United States. ⁴U.S. Naval Research Laboratory, 4555 Overlook Ave., SW, Washington, D.C., 20375, United States. ⁵Department of Biology, Monmouth University, West Long Branch, NJ, 07764, United States. ⁶Smithsonian Institution, Smithsonian Environmental Research Center, 647 Contees Wharf Road, Edgewater, Maryland, 21037, United States. ⁷Institute of Marine Sciences, University of North Carolina at Chapel Hill, 3431 Arendell Street, Morehead City, North Carolina, 28557, United States. *email: lharding@atmos.ucla.edu

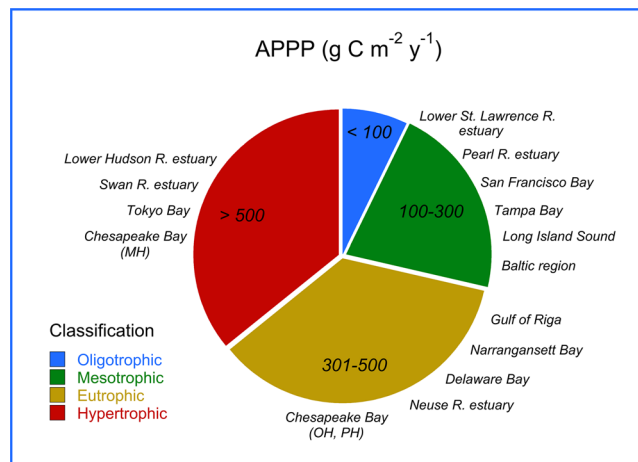


Figure 1. Trophic classification presented by Nixon (1995) based on APPP (g C m⁻² y⁻¹) including examples for selected estuarine-coastal ecosystems⁴.

in understanding phytoplankton dynamics in estuarine-coastal ecosystems followed a Chapman Conference of the American Geophysical Union (AGU) convened in Rovinj, Croatia in 2004, culminating in comprehensive global syntheses that highlighted long-term trends of biomass, floral (=taxonomic) composition, and APPP^{2,4-6}.

Nearly 20 years ago, we published depth-integrated models of net and gross primary production (NPP, GPP) for Chesapeake Bay (Fig. 2)⁷. These models were based on an approach by Behrenfeld and Falkowski⁸, the Vertically Generalized Production Model (VGPM), calibrated with long-term measurements of ¹⁴C-assimilation in the bay from 1982 to 2004⁷. Spatial, seasonal, and inter-annual variability of NPP and GPP in the bay was not well-defined prior to our studies, limiting the ability to resolve inter-annual variability of APPP⁹⁻¹⁵. We recently quantified climatic effects on water-quality properties including *chl-a*, Secchi depth, and oxidized nitrogen (nitrite plus nitrate = NO₂ + NO₃) using statistical models with terms for freshwater flow, salinity, and nutrient loadings to distinguish variability from long-term trends¹⁶⁻¹⁸. Here, we apply a similar approach to NPP and GPP, leading to improved spatio-temporal resolution of APPP sufficient to resolve inter-annual variability.

Recognition of eutrophication as a pressing issue in Chesapeake Bay stimulated individual studies dating to the 1970s⁹⁻²⁶, and long-term monitoring of water-quality properties initiated in the mid-1980s (Chesapeake Bay Program, US Environmental Protection Agency, <http://www.chesapeakebay.net>). Combined results define an annual cycle of phytoplankton biomass dominated by a spring bloom of centric diatoms following the winter-spring freshet of the Susquehanna River, with integrated, water-column chlorophyll-*a* (*chl-a*) reaching ~1000 mg m⁻² from April to mid-May. North-south gradients of light and nutrients driven by freshwater discharge deliver buoyancy, nutrients, and suspended particulate matter to the bay, strongly affecting the timing, position, and magnitude of the spring bloom, as reviewed by Malone¹⁴.

Seasonal warming leads to sea-surface temperatures (SST) ranging from 18 to 20 °C by late spring to early summer as persistent density stratification sets up. Deposition of organic material originating from the spring-bloom provides the substrate to fuel microbial metabolism, eventually leading to depletion of dissolved oxygen (DO) beneath the pycnocline, and regeneration of nutrients to support maximum NPP in summer. A transition in the phytoplankton community occurs from May to June following the sinking of spring-bloom diatoms, with a decrease of integrated, water-column *chl-a* to <200 mg m⁻²¹⁴. The summer flora is primarily composed of smaller, <20 μm diatoms, flagellated cells, including dinoflagellates, chrysophytes, cryptophytes, and non-motile picoplankton, such as cyanobacteria and other small, <3 μm cells, supporting the annual maximum of NPP from July to August^{27,28}.

Nutrient over-enrichment of the bay led to a 5- to 10-fold increase of surface *chl-a* for the polyhaline (PH) salinity zone, and a 1.5- to 2-fold increase for oligohaline and mesohaline (OH, MH) salinity zones from the 1950s to the 1990s^{20,21}. These increases were stimulated by eutrophication after World War II, evident in upward “trajectories” of total nitrogen (TN) and NO₂ + NO₃ loadings^{29,30}. Seasonal and inter-annual variability of freshwater discharge underlies spatio-temporal variability of water-quality properties, superimposed on historical changes and complicating the detection of long-term trends. We used statistical models to distinguish the eutrophication signal from variability associated with climatic effects, documenting the doubling of flow-adjusted TN and NO₂ + NO₃ loadings from 1945 to the early 1980s¹⁶⁻¹⁸. Newer studies followed this approach to adjust for climatic effects on water quality, phytoplankton biomass, floral composition, and NPP¹⁶⁻¹⁹.

Despite numerous studies of plankton ecology in Chesapeake Bay, limited spatio-temporal resolution of NPP and GPP restricts our ability to define inter-annual variability of APPP. To address this limitation, we developed statistical models of NPP and GPP based on earlier depth-integrated models^{7,31}, including an expanded set of predictor variables to account for nutrient loading and climatic effects on hydrology¹⁶⁻¹⁸. Principal goals were: (1) to develop predictive models of NPP and GPP calibrated to source data (1982 to 2004); (2) to apply the models to historical (1960s, 1970s) and monitoring (1985 to 2015) data with adjustments for nutrient loadings and climatic effects; (3) to estimate APPP from model predictions of NPP; (4) to test effects of simulated 40% reductions

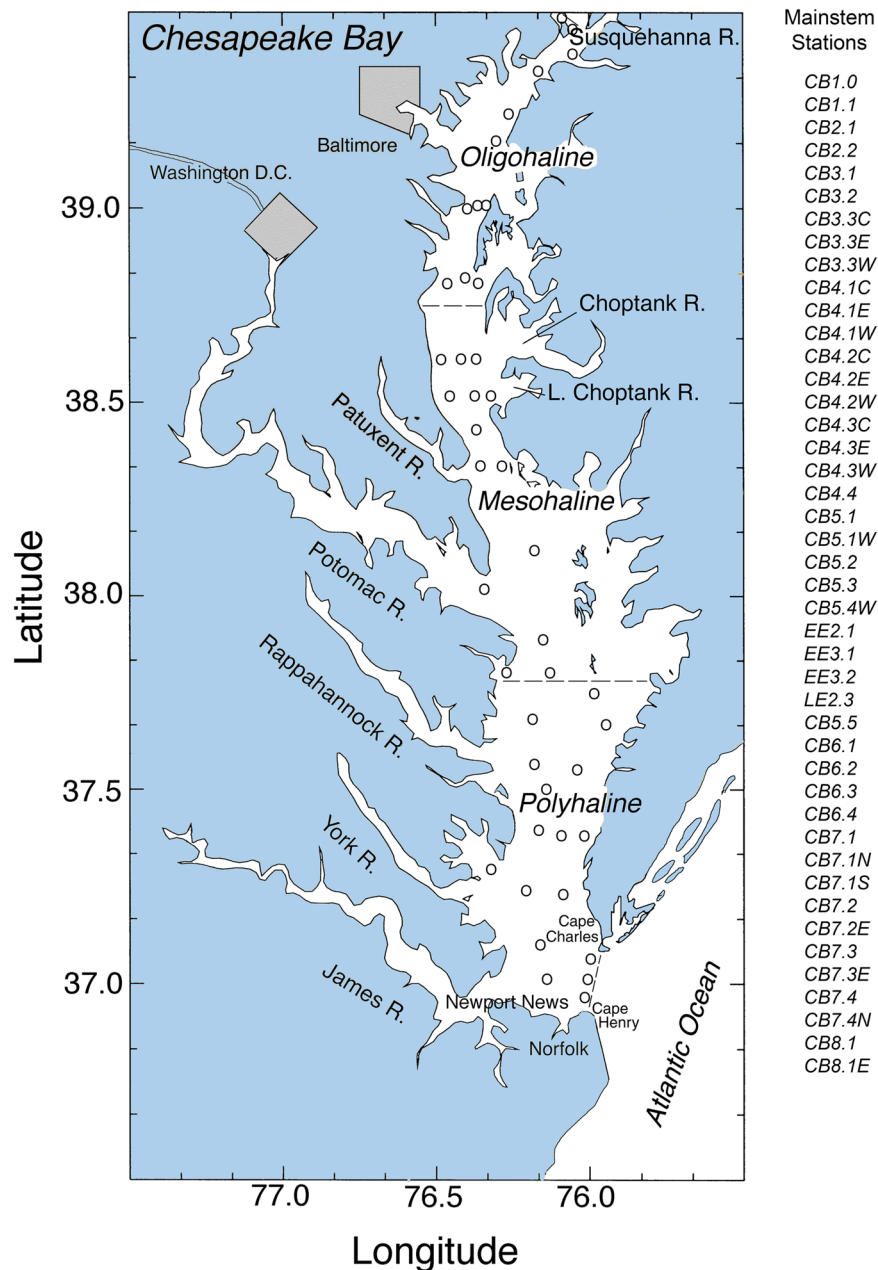


Figure 2. Map of study site showing major rivers, cities, salinity zones, and water-quality sampling stations in Chesapeake Bay.

of phytoplankton biomass or nutrient loadings on trophic classification based on APPP. Targeting these goals allowed us to test the hypothesis that nutrient reductions adopted by Chesapeake Bay jurisdictions would lead to reduced APPP and a change of trophic classification.

Methods

Cruises. Data were collected on 78 cruises on four research vessels from March 1982 to November 2004. All stations we occupied to measure NPP and GPP are depicted in Fig. 1. Data from a subset of these cruises were analyzed previously⁷. Experimental protocols for measuring NPP and GPP were specific to individual projects identified by acronyms in Table 1. CB cruises (1982–83) consisted of an initial transect for horizontal mapping to determine salinity, temperature, *chl-a*, nutrient, and turbidity gradients and to select stations for measuring NPP. ProPhot and FITS cruises (1987–88) and LMER PROTEUS cruises (1989–94) occupied stations along a north-south transect to map water-quality properties and to measure NPP and ancillary properties. NASA cruises (1993–94) occupied three stations per cruise in the lower bay, plume, and adjacent shelf waters interspersed with mapping legs to measure NPP, GPP, and ancillary properties. LMER TIES cruises (1995–2000) sampled stations at 0.5° latitudinal increments, and additional stations lateral to the north-south axis, for a total of nine to 27 stations per cruise. LMER TIES cruises also included legs for horizontal and vertical mapping, *in-situ* sampling of

Cruise	Research Vessel	Date	Cruise	Research Vessel	Date
CB-1	<i>Cape Hatteras</i>	Mar-82	NASA 94-02	<i>Cape Henlopen</i>	Apr-94
CB-2	<i>Cape Hatteras</i>	Jun-82	LMER 94-02	<i>Cape Henlopen</i>	Apr-94
CB-3	<i>Cape Hatteras</i>	Nov-82	LMER 94-05	<i>Cape Henlopen</i>	Jul-94
CB-4	<i>Cape Hatteras</i>	Mar-83	NASA 94-05	<i>Aquarius</i>	Jul-94
ProPhot-23	<i>Ridgely Warfield</i>	Apr-87	LMER 94-08	<i>Cape Henlopen</i>	Oct-94
ProPhot-24	<i>Ridgely Warfield</i>	May-87	TIES 98-01	<i>Cape Henlopen</i>	Apr-98
FITS-13	<i>Ridgely Warfield</i>	Jul-87	TIES 98-02 bp	<i>Cape Henlopen</i>	Jul-98
FITS-15	<i>Ridgely Warfield</i>	Aug-87	TIES 98-02	<i>Cape Henlopen</i>	Aug-98
ProPhot-25	<i>Ridgely Warfield</i>	Mar-88	TIES 98-03	<i>Cape Henlopen</i>	Oct-98
ProPhot-26	<i>Ridgely Warfield</i>	Apr-88	TIES 99-01	<i>Cape Henlopen</i>	Apr-99
ProPhot-27	<i>Ridgely Warfield</i>	May-88	TIES 99-02	<i>Cape Henlopen</i>	Jun-99
LMER 89-1	<i>Cape Henlopen</i>	Feb-89	TIES 99-02raz	<i>Cape Henlopen</i>	Jul-99
LMER 89-2	<i>Cape Henlopen</i>	Mar-89	TIES 99-02 bp	<i>Cape Henlopen</i>	Jul-99
LMER 89-3	<i>Cape Henlopen</i>	Apr-89	TIES 99-03	<i>Cape Henlopen</i>	Oct-99
LMER 89-4	<i>Cape Henlopen</i>	May-89	TIES 00-01	<i>Cape Henlopen</i>	Apr-00
LMER 89-5	<i>Cape Henlopen</i>	Jun-89	TIES 00-02	<i>Cape Henlopen</i>	Jul-00
LMER 89-6	<i>Cape Henlopen</i>	Jul-89	TIES 00-03	<i>Cape Henlopen</i>	Oct-00
LMER 89-7	<i>Cape Henlopen</i>	Aug-89	BIO 01-01	<i>Cape Henlopen</i>	Apr-01
LMER 89-8	<i>Cape Henlopen</i>	Sep-89	BIO 01-02	<i>Cape Henlopen</i>	Aug-01
LMER 89-9	<i>Cape Henlopen</i>	Nov-89	BIO 01-03	<i>Cape Henlopen</i>	Oct-01
LMER 90-3	<i>Cape Henlopen</i>	Apr-90	BIO 02-01	<i>Cape Henlopen</i>	Apr-02
LMER 90-4	<i>Cape Henlopen</i>	Apr-90	BIO 02-02	<i>Cape Henlopen</i>	Jul-02
LMER 90-5	<i>Cape Henlopen</i>	May-90	BIO 02-03	<i>Cape Henlopen</i>	Oct-02
LMER 90-6	<i>Cape Henlopen</i>	May-90	BIO 03-01	<i>Cape Henlopen</i>	Apr-03
LMER 90-7	<i>Cape Henlopen</i>	Jul-90	MOVE 08-03	<i>Cape Henlopen</i>	Aug-03
LMER 90-8	<i>Cape Henlopen</i>	Aug-90	BIO 03-02	<i>Cape Henlopen</i>	Oct-03
LMER 90-11	<i>Cape Henlopen</i>	Nov-90	SGER 11-03	<i>Cape Henlopen</i>	Nov-03
LMER 91-3	<i>Cape Henlopen</i>	Apr-91	ACE 04-01	<i>Cape Henlopen</i>	Apr-04
LMER 91-4	<i>Cape Henlopen</i>	May-91	BIO 04-01	<i>Cape Henlopen</i>	Apr-04
LMER 91-6	<i>Cape Henlopen</i>	Jul-91	ACE 04-02	<i>Cape Henlopen</i>	Apr-04
LMER 91-7	<i>Cape Henlopen</i>	Aug-91	ACE 04-02B	<i>Cape Henlopen</i>	May-04
LMER 91-9	<i>Cape Henlopen</i>	Sep-91	ACE 04-03B	<i>Cape Henlopen</i>	May-04
LMER 91-10	<i>Cape Henlopen</i>	Oct-91	ACE 04-04	<i>Cape Henlopen</i>	Jun-04
LMER 91-11	<i>Cape Henlopen</i>	Oct-91	ACE 04-04B	<i>Cape Henlopen</i>	Jun-04
LMER 91-11	<i>Cape Henlopen</i>	Oct-91	ACE 04-04 C	<i>Cape Henlopen</i>	Jul-04
LMER 92-03	<i>Cape Henlopen</i>	Apr-92	BIO 04-02	<i>Cape Henlopen</i>	Jul-04
LMER 92-06	<i>Cape Henlopen</i>	Jul-92	ACE 04-05	<i>Cape Henlopen</i>	Aug-04
LMER 92-09	<i>Cape Henlopen</i>	Oct-92	ACE 04-06	<i>Cape Henlopen</i>	Aug-04
LMER 93-06	<i>Cape Henlopen</i>	Oct-93	BIO 04-03	<i>Cape Henlopen</i>	Sep-04

Table 1. Summary of cruises, research vessels, and dates for measurements of ^{14}C -assimilation in simulated *in-situ* incubations for samples collected at 716 stations on 78 cruises from 1982 to 2004.

phytoplankton, zooplankton, and fish, towed-body sampling with an instrumented SCANFISH (Geological & Marine Instrumentation), and continuous underway measurements of water-quality properties using the ship's Serial ASCII Instrumentation Loop (SAIL) system. EPA, NASA, and NSF cruises (2001–2004) used the same protocols as TIES cruises.

Horizontal transects. Continuous underway sampling on horizontal transects was used to characterize distributions of water-quality properties. Some methods used on horizontal transects were described previously⁷. Instrumentation was specific to the vessel used. For CB, ProPhot, and FITS cruises on the *Cape Hatteras* and *Ridgely Warfield* (1982–1988), discrete samples were spaced 4–5 km along transects. Yellow Springs Instruments model 33 salinometer and model 57 oxygen meter were used for mapping on CB cruises on the *Cape Hatteras* (1982–1983). InterOcean, Inc. Inductive Conductivity and Temperature Indicator (ICTI) was used on ProPhot and FITS cruises on the *Ridgely Warfield* (1987–1988). The NASA cruise on the *Aquarius* (1994) used a SeaBird conductivity-temperature-depth-fluorescence-oxygen instrument package (CTDFO₂) in pump-through mode. NSF LMER PROTEUS, TIES, and NASA, Biocomplexity, and SGER cruises on the *Cape Henlopen* (1989–2004) used the ship's flow-through SAIL system for surface mapping, with SeaBird sensors for salinity and temperature, and Turner Designs model 10 fluorometers for *chl-a* and turbidity. Instrument readings were calibrated for all transects using periodic grab samples.

Vertical profiles. Vertical profiles of salinity, temperature, dissolved oxygen (DO), and *chl-a* fluorescence were determined from hydro-casts at a set of stations spaced 10–20 km along horizontal transects. Some of the methods to obtain vertical profiles of these properties were described previously⁷. Hydrocasts were made with Yellow Springs salinity and DO meters (see above) on 1982–1983 cruises, a Sea Bird model 9 CTDFO₂ on 1987–1988 cruises, and a Neil Brown Mark III CTDFO₂ on 1989–2004 cruises. Discrete samples were collected in Niskin bottles to calibrate fluorometers and DO meters. Surface sunlight during the day (E_0 = downwelling irradiance, photosynthetically available radiation = PAR) was measured with a Li-Cor quantum meter model 190 S (or equivalent) coupled to a Li-Cor model 550 or 1000 integrator. The sensor was mounted near the deck incubators we used to measure simulated *in-situ* NPP and GPP. Diffuse light attenuation coefficient for PAR (K_{PAR}) was determined from vertical profiles with a submersible Li-Cor quantum meter model 188B with a 192S sensor or equivalent for CB, ProPhot, FITS, and LMER PROTEUS, TIES, and NASA cruises. Secchi depths (m) were determined for all stations and cruises. Euphotic-layer depth (Z_p) was estimated as the depth to which 1% of E_0 penetrated based on vertical profiles of downwelling irradiance (E_d), or from Secchi depth using calibration regressions³². NSF LMER TIES and NASA cruises also conducted vertical profiles with a Biospherical Instruments multi-spectral environmental radiometer (MER-2040/41) to measure K_{PAR} and spectral light attenuation.

Water-quality properties. *Chl-a* was determined using spectrophotometric and fluorometric measurements on acetone extracts (90%) of particulate material collected by vacuum filtration onto glass-fiber filters (Whatman GF/F or equivalent, 0.3–0.8 μ m nominal pore sizes). Spectrophotometric *chl-a* was derived from trichromatic equations applied to absorbances measured on a Beckman DK-2 or equivalent, and fluorometric *chl-a* was measured on a Turner model 110, 111, or Turner Designs model 10 calibrated by spectrophotometry^{20,21}. Secchi depth was the depth at which a 30-cm white disk became invisible when lowered over the side of the research vessel. $NO_2 + NO_3$ was measured using analytical methods documented by the EPA/CBP^{33,34} following protocols described by D'Elia *et al.*³⁵.

Simulated *in-situ* incubations. NPP was measured at 723 stations from 1982 to 2004, and GPP at 525 stations from 1995 to 2004. Whole-water samples were collected in Niskin bottles mounted on a rosette sampler at sunrise at a depth of 0.5 to 1.0 m, contents were pooled in a darkened carboy, and dispensed to 125–150 ml glass incubation bottles. The euphotic layer is well mixed in the bay and *chl-a* is homogeneously distributed in the upper 5–10 m. NPP and GPP were determined using ¹⁴C-sodium bicarbonate uptake in deck incubators cooled with flowing surface water (± 1 °C of *in-situ* temperatures). 2 to 5 μ Curies of ¹⁴C-sodium bicarbonate (ICN Pharmaceuticals, Inc., or Amersham Searle, Inc.) were added to each incubation bottle. Total ¹⁴C-sodium bicarbonate activity was determined for a time-zero aliquot from one of the incubation bottles, and from a small amount of stock isotope added to scintillation cocktail made basic with NaOH (Aquasol, New England Nuclear, Inc., or equivalent). Incubation bottles were exposed to a range of sunlight levels using neutral density screens providing 100 (no screens), 58, 34, 21, 11, 4 and 1% transmission to simulate seven depths in the euphotic layer. Dark uptake was measured in an opaque bottle and used as a tare value to adjust uptake in illuminated bottles.

NPP on cruises from 1982 to 1983 was measured in 3–4 h incubations repeated four times during the photoperiod, with additional bottles incubated throughout the night. NPP on cruises from 1987 to 2004 was measured in 24-h incubations, and GPP on cruises from 1995 to 2004 was measured in 4–6 h incubations. Concurrent measurements using ¹⁴C and O₂ methodologies confirmed this approach accurately estimated NPP and GPP⁷. Duplicate 25–150 ml subsamples (depending on phytoplankton biomass) were withdrawn at the end of these periods and filtered onto glass fiber filters (Gelman AE or Whatman GF/F) under low vacuum pressure (<150 mm Hg). Filter pads were rinsed with filtered water of equivalent salinity as the sample and acidified with 0.01 N HCl in a fume hood to remove residual inorganic label. Activities were determined on a Packard Instruments Tri-Carb or model 3320 liquid scintillation counter. Duplicate aliquots were withdrawn from incubation bottles to determine *chl-a* using methods described above. Total CO₂ was measured by gas-stripping, capture, and analysis on a Beckman model 864 infrared analyzer for 1982–83 cruises, Gran titration for 1987–1988 cruises, and by gas chromatography on a Hach Cable Series 100 AGC for 1989–2004 cruises.

Computations of NPP and GPP. Equations to compute NPP and GPP combined terms for ¹⁴C-uptake in lighted bottles tared against non-photosynthetic ¹⁴C-uptake in dark bottles, divided by the total ¹⁴C activity added, and multiplied by a discrimination factor of 1.05 for ¹⁴C vs ¹²C and a term for total CO₂ (mM) converted to weight (mg m⁻³). The resulting volumetric rates (PP, mg C m⁻³ h⁻¹) were used to compute NPP and GPP by converting simulated incubation depths as percent surface irradiance (E_0) to actual depths based on K_{PAR} from vertical profiles of irradiance (E_d) or Secchi depth. Multiple-segment trapezoidal integration was applied to PP from the surface to euphotic-layer depth to obtain NPP and GPP. NPP was determined from 24-h incubations and GPP from 4–6 h incubations scaled to the photoperiod using E_0 during incubations as a proportion of total E_0 for the day. Optimal photosynthesis, P^B_{opt} , was determined as maximum PP in simulated *in-situ* incubations normalized to *chl-a*. Observed values of $\log_{10} P^B_{opt}$ were binned in 1° increments as a function of SST following the approach of Son *et al.*³¹ and analyzed by polynomial regression. Estimates of $\log_{10} P^B_{opt}$ from these regressions were used as model inputs to predict NPP for historical (1960s, 1970s) and monitoring (1985–2015) programs.

Freshwater discharge, climatic effects. Daily freshwater discharge from the Susquehanna River (SRF) and monthly cumulative discharge (SUM) were obtained from the U.S. Geological Survey (USGS) (<http://md.water.usgs.gov>) for the Conowingo Dam gaging station near the head of the bay (latitude 39° 39' 28.4", longitude 76° 10' 28.0"). TN and $NO_2 + NO_3$ loadings were obtained as monthly values (10⁶ kg) from the USGS. We focused on the Susquehanna River as this large river dominates distributions of nutrients and phytoplankton in the main stem bay. Nutrient loadings from other tributaries are significantly reduced by processes within their confines,

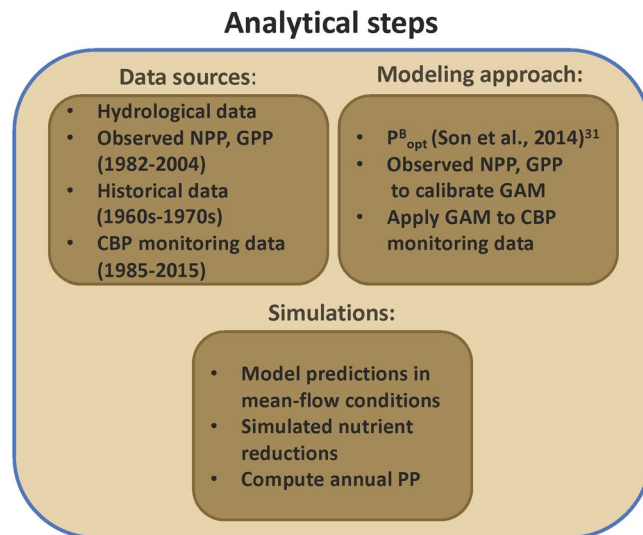


Figure 3. Summary of analytical steps including data sources, modeling approach, and simulations.

attenuating effects of lateral inputs on the bay proper^{16–18}. Climatic effects were quantified by applying GAM to input files for NPP, GPP, and water-quality properties, including terms for freshwater flow (\log_{10} monthly SRP, \log_{10} monthly SUM) and salinity. Model predictions of NPP and GPP for low-flow, “dry” conditions were based on flow terms set at 10th percentiles joined by salinity terms at 90th percentiles; mean-flow model predictions were based on flow and salinity terms held constant at their mean values; model predictions for high-flow, “wet” conditions were based on flow terms set at 90th percentiles joined by salinity terms at 10th percentiles.

Analytical steps. A flow-chart of analytical steps, including data sources, modeling approach, and simulations is presented in Fig. 3. Statistical analyses were conducted using “R” v. 3.6.0. Non-linear fits of time-series data were developed using GAM from the “R” package ‘mgcv’, containing functions similar to those designed by T. Hastie in S-Plus, and based on a penalized regression-spline approach including automatic smoothness selection^{36–38}. Model predictions of NPP and GPP were adjusted for climatic effects using GAM, as described previously for water-quality properties^{16–19}. A comparable approach by Beck and Murphy³⁹ compared GAM to weighted regressions of time, discharge and season (WRTDS) developed by Hirsch *et al.*⁴⁰, noting the flexibility of GAM to add relevant predictor variables as a strength of GAM over alternatives.

Model fits, residuals, flow-adjusted model predictions at monthly increments, adjusted R^2 , generalized cross validation (GCV) score, % deviance explained, p-values for F-statistics, and root mean square error (RMSE) were obtained for each model. Degrees of smoothing (knots = k) were selected by the “R” package ‘mgcv’ to minimize the GCV score, followed by post-hoc adjustments of “k” for individual terms using the function ‘gam.check’. Graphical presentations were prepared with Kaleidagraph 4.5.2 (Synergy Software, Inc.). These include time series of mean, monthly NPP and euphotic-layer *chl-a* (Fig. 4a–c), polynomial regressions of P^B_{opt} on SST (Fig. 5a,b), observed vs model-fitted values of \log_{10} NPP and \log_{10} GPP (Fig. 6a–f), probability distributions of observed and predicted \log_{10} NPP and \log_{10} GPP (Fig. 7a–d), comparisons of predicted \log_{10} NPP from gam1 and gam2 (Fig. 8a–c), time-series of \log_{10} *chl-a*, \log_{10} euphotic-layer *chl-a*, and model predictions of \log_{10} NPP from 1985 to 2015 (Fig. 9a–i), flow-adjusted model predictions of \log_{10} euphotic-layer *chl-a* and \log_{10} NPP for low-flow, mean-flow, and high-flow conditions (Fig. 10a–f), time series of APPP based on mean-flow model predictions of NPP and simulated reductions of euphotic-layer *chl-a* or TN and $\text{NO}_2 + \text{NO}_3$ loadings, and observed euphotic-layer *chl-a* (Fig. 11a–c), and historical reconstructions of mean, monthly \log_{10} NPP and \log_{10} *chl-a* for the 1960s and 1970s with estimates of APPP (Fig. 12a–f).

Results

Annual cycles. Spatial and seasonal differences were evident in mean, monthly euphotic-layer *chl-a* and NPP based on shipboard measurements in Chesapeake Bay from 1982 to 2004 (Fig. 4a–c). Seasonal maxima of phytoplankton biomass and production occurred in summer for the OH salinity zone, with euphotic-layer *chl-a* $\sim 40 \text{ mg m}^{-2}$ and NPP $\sim 1200 \text{ mg C m}^{-2} \text{ d}^{-1}$ in July and August (Fig. 4a). Contrasting patterns for the MH salinity zone consisted of a well-developed spring bloom with euphotic-layer *chl-a* $> 80\text{--}100 \text{ mg m}^{-2}$ in April and May, displaced several months from a summer maximum of NPP $> 2000 \text{ mg m}^{-2} \text{ d}^{-1}$ in July (Fig. 4b). A second maximum of euphotic-layer *chl-a* from $60\text{--}80 \text{ mg m}^{-2}$ occurred in fall for the MH salinity zone but was not matched by a maximum of NPP (Fig. 4b). Annual cycles of euphotic-layer *chl-a* and NPP for the PH salinity zone were similar in profile and somewhat lower compared to those for the MH salinity zone, with maxima of euphotic-layer *chl-a* $\sim 60 \text{ mg m}^{-2}$ and NPP $\sim 1700 \text{ mg m}^{-2} \text{ d}^{-1}$ in May and September, respectively (Fig. 4c). Table 2 summarizes the statistical properties of shipboard measurements from 1982 to 2004 by salinity zone and season, including Z_p , salinity, SST, surface *chl-a*, euphotic-layer *chl-a*, NPP, and GPP.

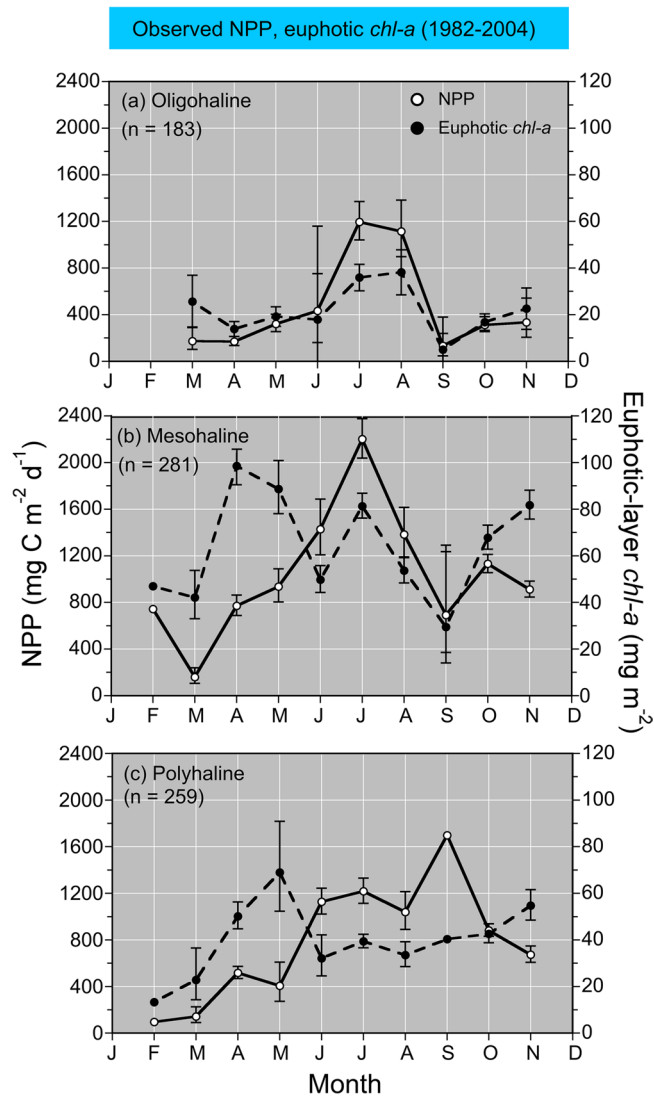


Figure 4. (a–c) Mean, monthly (\pm SE) observed NPP ($\text{g C m}^{-2} \text{d}^{-1}$) (left ordinate) and euphotic-layer *chl-a* (mg m^{-2}) (right ordinate) for oligohaline (OH), mesohaline (MH), and polyhaline (PH) salinity zones.

Models of $P_{\text{opt}}^{\text{B}}$, NPP, and GPP. $P_{\text{opt}}^{\text{B}}$ was estimated from third-order polynomial regressions of observed $\log_{10} P_{\text{opt}}^{\text{B}}$ on binned SST as described by Son *et al.*³¹. These regressions had $p < 0.001$ and $R^2 > 0.80$ (Fig. 5a,b). Estimates of $\log_{10} P_{\text{opt}}^{\text{B}}$ from these regressions were combined with input data on water-quality properties to predict NPP and GPP. Table 3 presents a complete list of predictor variables for models of NPP and GPP. Simple, linear regressions of observed vs model-fitted \log_{10} NPP and GPP had $p < 0.001$ for OH, MH, and PH salinity zones (Table 4; Fig. 6a–f). Probability distributions of observed and model-fitted \log_{10} NPP and GPP confirmed that the models generated unbiased estimates as model predictions displayed statistical attributes indistinguishable from observations (Fig. 7a–d).

Model predictions. Five GAM formulations were developed to accommodate estimates of \log_{10} NPP and \log_{10} GPP based on availability of data for predictor variables in different time periods (Table 5). We focused primarily on model predictions of \log_{10} NPP as these supported estimates of APPP. Model predictions of \log_{10} NPP were compared for gam1 and gam2, i.e., model formulations with and without the predictor variable “sequential year” (Seq_year). By omitting Seq_year in gam2, we avoided an assumption that long-term trends in calibration data (1982 to 2004) were unchanged for water-quality properties outside that range (2005 to 2015) that were used to predict \log_{10} NPP. Both gam1 and gam2 captured seasonal to interannual variability of \log_{10} NPP, with differences in long-term trends expressed in simple, linear regressions of model predictions on year (Fig. 8a–c). Subsequent analyses predicted \log_{10} NPP from 1985 to 2015 using gam2 based on water-quality properties as data inputs. An alternate model to gam2 was developed as gam3 to address data limitations for historical periods, using the term $\log_{10} \text{chl-a}$ for biomass in place of \log_{10} euphotic-layer *chl-a*. gam3 was further modified to gam4 by omitting the term K_{PAR} and to gam5 by omitting the term for season. These models were applied to input data from the 1960s and 1970s as \log_{10} euphotic-layer *chl-a*, K_{PAR} , or season were either absent or too sparse to support model predictions with reasonable sample sizes.

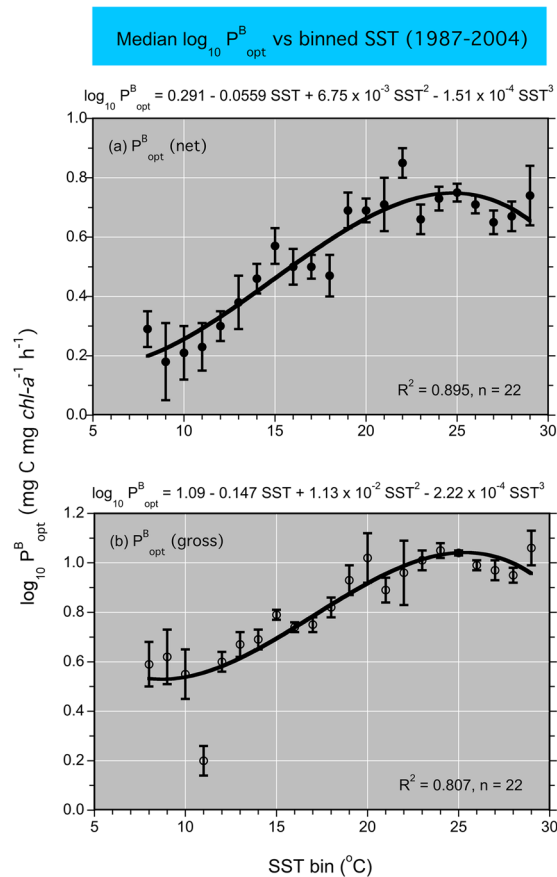


Figure 5. (a,b) Relationships of $\log_{10} P_{opt}^B$ (net) and (gross) to binned sea-surface temperature (SST). Time-series observations included additional measurements from 2002 to 2004 to update three-order polynomial regressions of Son *et al.*³¹.

Water-quality time series. Observed mean, monthly $\log_{10} chl-a$ (mg m^{-3}) (Fig. 9a–c), \log_{10} euphotic-layer $chl-a$ (mg m^{-2}) (Fig. 9d–f), and model predictions of \log_{10} NPP ($\text{mg C m}^{-2} \text{ d}^{-1}$) (Fig. 9g–i) are presented for OH, MH, and PH salinity zones from 1985 to 2015. Corresponding statistical properties for these water-quality data are compiled in Table 6. Simple, linear regressions showed upward trends of $\log_{10} chl-a$ for OH and MH salinity zones (Fig. 9a,b), but no trend for the PH salinity zone (Fig. 9c); \log_{10} euphotic-layer $chl-a$ showed upward trends for OH, MH, and PH salinity zones (Fig. 9d–f); \log_{10} NPP increased for OH and MH salinity zones (Fig. 9g,h), and decreased for the PH salinity zone (Fig. 9i).

Climatic effects. Climatic effects on \log_{10} euphotic-layer $chl-a$ and \log_{10} NPP are expressed as model predictions for low-flow, “dry”, mean-flow, and high-flow, “wet” conditions for OH, MH, and PH salinity zones from 1985 to 2015 (Fig. 10a–f). Simple, linear regressions showed consistent upward trends of \log_{10} euphotic-layer $chl-a$ for all three salinity zones (Fig. 10a–c). Low-flow conditions did not affect \log_{10} euphotic-layer $chl-a$ for the OH salinity zone but led to decreased \log_{10} euphotic-layer $chl-a$ for MH and PH salinity zones. High-flow conditions led to decreased \log_{10} euphotic-layer $chl-a$ for the OH salinity zone, did not affect \log_{10} euphotic-layer $chl-a$ for the MH salinity zone, and led to increased \log_{10} euphotic-layer $chl-a$ for the PH salinity zone. NPP was less sensitive to climatic effects than euphotic-layer $chl-a$, documented as time series of \log_{10} NPP for low-flow, mean-flow, and high-flow conditions (Fig. 10d–f). Simple, linear regressions of mean-flow predictions of \log_{10} NPP showed upward trends for OH and MH salinity zones, but no trend for the PH salinity zone.

Euphotic-layer $chl-a$, APPP. Time series of mean, annual euphotic-layer $chl-a$ based on observations from 1985 to 2015 showed upward trends for OH and MH salinity zones, but not for the PH salinity zone (Fig. 11a–c). Corresponding APPP estimates from mean-flow model predictions of NPP showed upward trends from 1985 to 2015 for all three salinity zones. APPP ranged from ~ 200 to $300 \text{ g C m}^{-2} \text{ yr}^{-1}$ for the OH salinity zone, ~ 250 to $550 \text{ g C m}^{-2} \text{ yr}^{-1}$ for the MH salinity zone, and 280 to $350 \text{ g C m}^{-2} \text{ yr}^{-1}$ for the PH salinity zone. Using Nixon’s trophic classification³, APPP corresponded to “eutrophic” conditions for OH and PH salinity zones, and “hyper-trophic” conditions for the MH salinity zone. APPP based on mean-flow model predictions of NPP with simulated 40% reductions of euphotic-layer $chl-a$ or TN and $\text{NO}_2 + \text{NO}_3$ loadings showed reductions for all three salinity zones (Fig. 11a–c). These reductions of biomass or nutrient loadings changed APPP to mesotrophic conditions for OH and PH salinity zones, and to eutrophic conditions for the MH salinity zone.

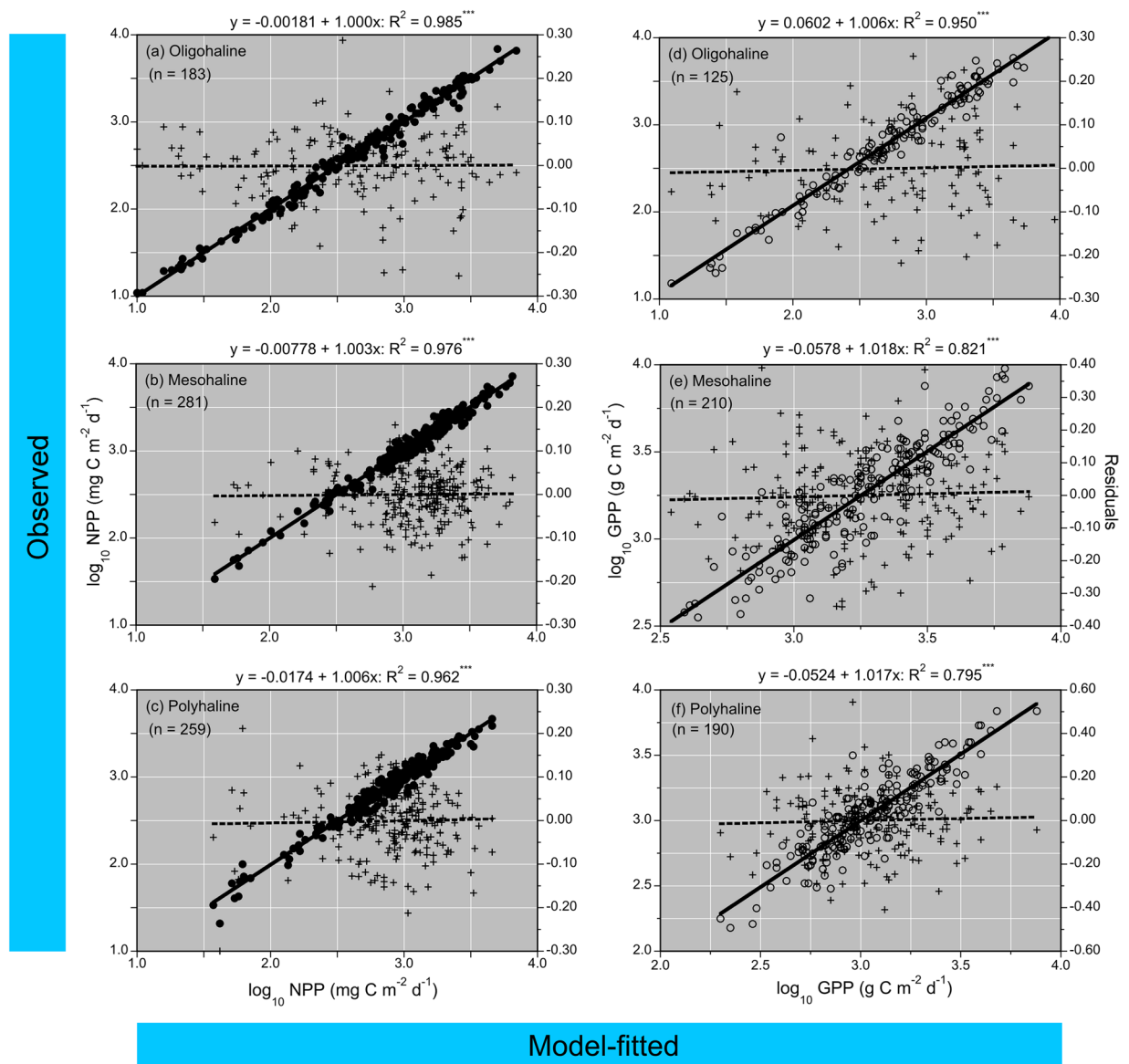


Figure 6. (a–f) Simple, linear regressions of observed vs predicted log₁₀ NPP and GPP (mg C m⁻² d⁻¹) for OH, MH, and PH salinity zones using generalized additive models (GAM). Source data for GAM were obtained in measurements of simulated *in-situ* ¹⁴C-bicarbonate assimilation and ancillary properties from 1982 to 2004 (n = 723). Closed circles = log₁₀ NPP; open circles = log₁₀ GPP; crosses = residuals, dashed lines = simple, linear regressions of residuals vs model-fitted NPP or GPP.

Historical reconstructions. Archival data on water-quality properties, including $P^{B_{opt}}$ from polynomial regressions on SST (Fig. 5a), log₁₀ *chl-a*, and other predictor variables (Table 3), supported model predictions of log₁₀ NPP in the 1960s and 1970s (Fig. 12a–f). Model predictions from gam4 supported historical reconstructions of log₁₀ NPP for low-flow, “dry”, mean-flow, and high-flow, “wet” conditions to capture climatic effects (Table 5). APPP based on mean-flow predictions of NPP for the OH salinity zone reached 555 g C m⁻² y⁻¹ in the 1960s, compared to 288 g C m⁻² y⁻¹ in the 1970s (Fig. 12a,d). APPP for MH and PH salinity zones showed similar patterns, ranging from 392 to 504 g C m⁻² y⁻¹ in the 1960s, and from 132 to 334 g C m⁻² y⁻¹ in the 1970s (Fig. 12b,c,e,f). Mean-flow predictions of log₁₀ NPP in the 1960s showed summer maxima for OH and MH salinity zones (Fig. 12a,b), while sparse data for the PH salinity zone limited resolution for that period (Fig. 12c). Observed log₁₀ *chl-a* showed summer maxima for OH, MH, and PH salinity zones, and an absence of a spring maximum for the MH salinity zone (Fig. 12b).

Discussion

NPP and GPP models. Important advances in NPP and GPP models for estuarine-coastal waters were made possible by increasingly sophisticated approaches and availability of calibration data. Common elements of production models dating to the 1950s include terms for photosynthetic efficiency, phytoplankton biomass, and light availability^{41–52}. Light-utilization models specific to estuarine-coastal ecosystems, such as Chesapeake Bay, San

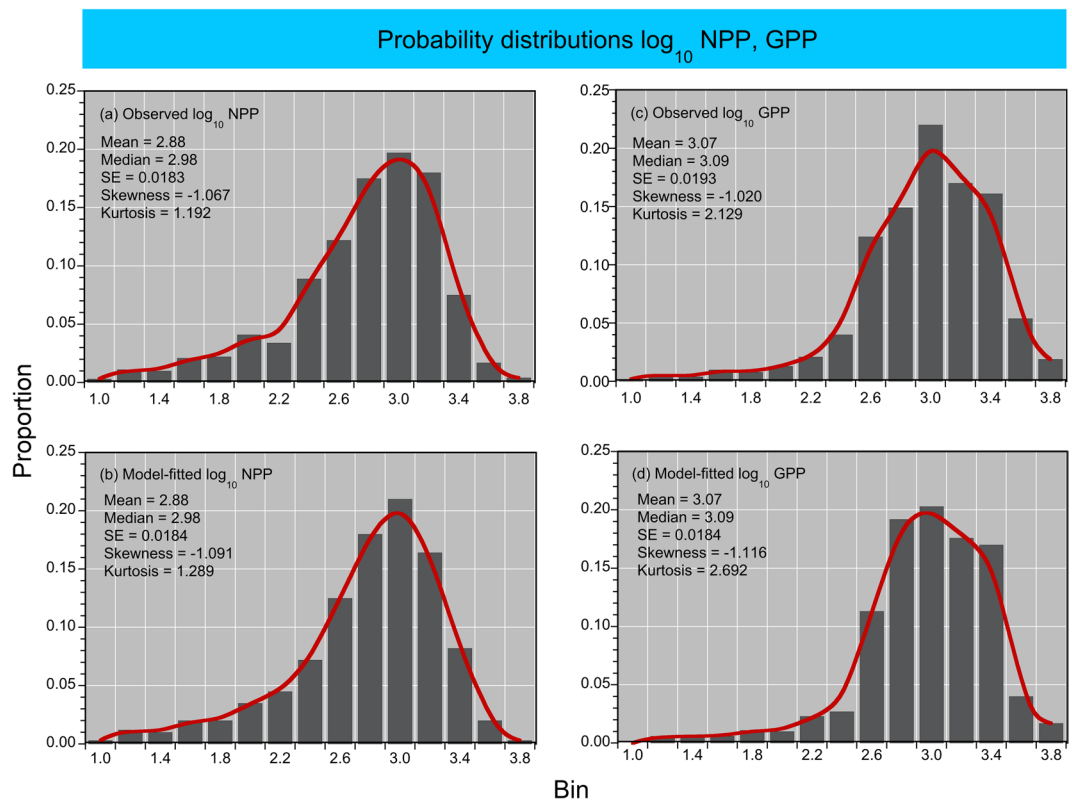


Figure 7. (a–d) Probability distributions of observed and predicted daily \log_{10} NPP and GPP ($\text{g C m}^{-2} \text{d}^{-1}$).

Francisco Bay, and mid-Atlantic coastal waters, relied on observations of euphotic-layer *chl-a*, incident irradiance (E_0), light attenuation coefficient (K_{PAR}), NPP, and GPP^{11,14,48–50}. In 1997, Behrenfeld and Falkowski developed VGPM, a depth-integrated model applied to ocean-color data from SeaWiFS (Sea-viewing Wide Field of View Sensor) and MODIS (Moderate Resolution Imaging Spectroradiometer) that provide global coverage of NPP⁸. In 2002, we developed the Chesapeake Bay Production Model (CBPM) as the published form of VGPM overestimated NPP and GPP for the bay⁷. Stepwise regressions of log-transformed variables from VGPM led to CBPM that supported estimates of NPP from aircraft and satellite ocean-color data^{31,53}.

Here, we departed from VGPM and CBPM to develop production models for the bay using GAM. Selection of predictor variables for NPP and GPP models was informed by earlier studies on a subset of these data from LMER TIES cruises (Table 1). Analysis of variance (ANOVA) showed that season and region explained most of the variability of phytoplankton properties, including NPP, *chl-a*, and floral composition⁵⁴. Long-term (six-year) means of NPP were negatively correlated with the fraction of *chl-a* in diatoms, a property stimulated by high-flow, “wet” conditions. Multiple linear regression and principal component analysis identified SRF as a ‘master variable’ driving inter-annual variability of these properties. An important advantage of transitioning to GAM was the flexibility to include predictor variables such as SRF to adjust for climatic effects on hydrology and distinguish variability from trends.

Model forms developed here were guided by these findings, leading us to include predictor variables for salinity zone, salinity, month, season, year, and flow terms \log_{10} SRF and \log_{10} SUM (Table 3). These models proved effective to estimate NPP and GPP, exemplified by simple, linear regressions of observed vs. modeled \log_{10} NPP from gam2 with $R^2 > 0.96$ (Fig. 6a–c), and \log_{10} GPP from gam2 with $R^2 > 0.80$ (Fig. 6d–f). These fits are comparable to NPP estimates using CBPM with measured values of $P_{\text{opt}}^{\text{B}}$, and GPP estimates using CBPM with estimated values of $P_{\text{opt}}^{\text{B}}$. Predictor variables in models of NPP for OH, MH, and PH salinity zones consistently showed highest F-values and lowest p-values for $\log_{10} P_{\text{opt}}^{\text{B}}$ and \log_{10} euphotic-layer *chl-a* (Table 3). Several other terms were also significant predictor variables, i.e., TN and $\text{NO}_2 + \text{NO}_3$ loadings (OH salinity zone), salinity, month (MH salinity zone), and salinity, K_{PAR} , SRE, and month (PH salinity zone).

Climatic effects. Our group has focused on climatic effects on hydrology impacting water quality and phytoplankton in recent studies of Chesapeake Bay^{16–19}. Adolf *et al.*⁵⁴ explored this theme previously, reporting predictable consequences of SRF on phytoplankton dynamics. Statistical models based on long-term data extended these findings, documenting climatic effects on *chl-a*, floral composition, and NPP^{16–19}. A logical sequence emerged from these studies wherein seasonal to interannual variability of freshwater flow and N loading regulates spatio-temporal distributions of phytoplankton^{16–19}, consistent with the conclusion by Malone *et al.*²² that P plays a limited, transient role in the OH salinity zone of the bay, while N limits phytoplankton biomass and production on the ecosystem scale.

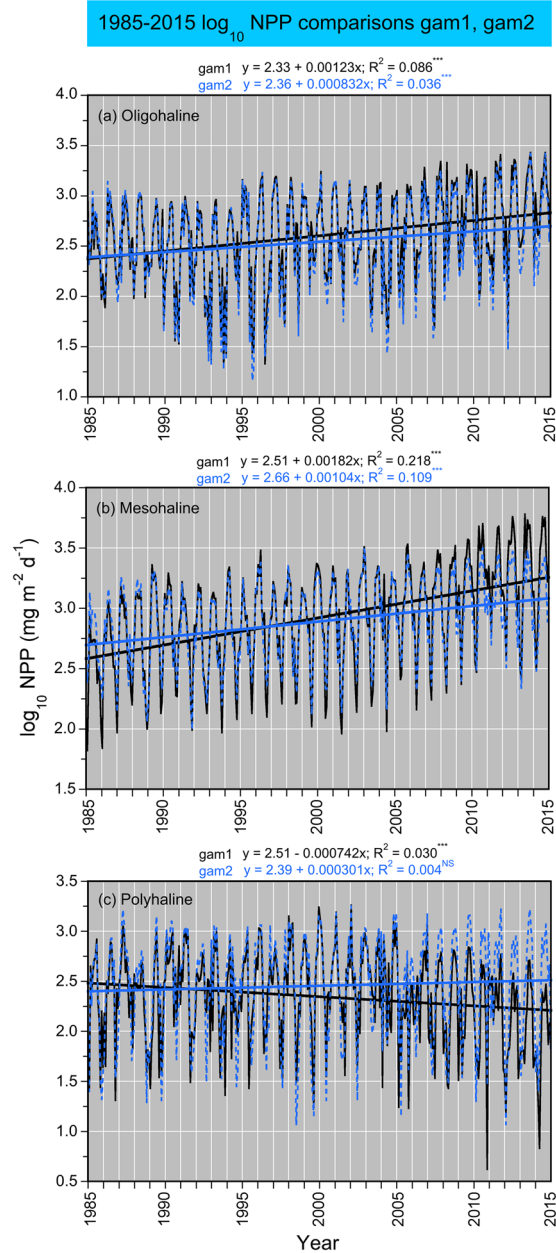


Figure 8. (a–c) Comparisons of \log_{10} NPP using predictions from generalized additive models (GAM) from 1985 to 2015; gam1 included a predictor variable for the time term “Seq-year” and gam2 omitted this variable (see Table 4).

Despite evidence from shipboard, aircraft, and satellite data linking freshwater flow to phytoplankton dynamics in land-margin ecosystems, previous NPP and GPP models did not contain explicit terms for climatic effects on hydrology^{12–14,51,52,54–60}. Analyses described here addressed this shortcoming, based on observations in Chesapeake Bay spanning several decades. Specifically, low-flow, “dry” conditions produce a landward shift of N-limitation toward OH and MH salinity zones, lower *chl-a*, lower NPP, and a lower proportion of diatoms in the phytoplankton flora; high-flow, “wet” conditions extend the area of N sufficiency seaward to MH and PH salinity zones, leading to higher *chl-a*, higher NPP, and a higher proportion of diatoms^{16–19,54,60}. Climatic effects on bio-optically active constituents similarly affect light-limitation as higher inputs of dissolved and suspended materials occur for high-flow, “wet” conditions than for low-flow, “dry” conditions^{16,18}. This latter observation may contribute to lower sensitivity of NPP than *chl-a* to climatic variability reported here (Fig. 10a–f).

Development of numerical water-quality criteria followed this logic, leading to model predictions that distinguished long-term trends from spatio-temporal variability¹⁸. Freshwater flow from the Susquehanna River, and frequencies of predominant weather patterns defined “dry” and “wet” conditions^{53,60–62}, and statistical models conditioned on specific input terms for flow and salinity supported predictions of mean, monthly *chl-a*, Secchi depth, and $\text{NO}_2 + \text{NO}_3$ ¹⁹. Here, we extended this approach to NPP and GPP models by including terms to adjust

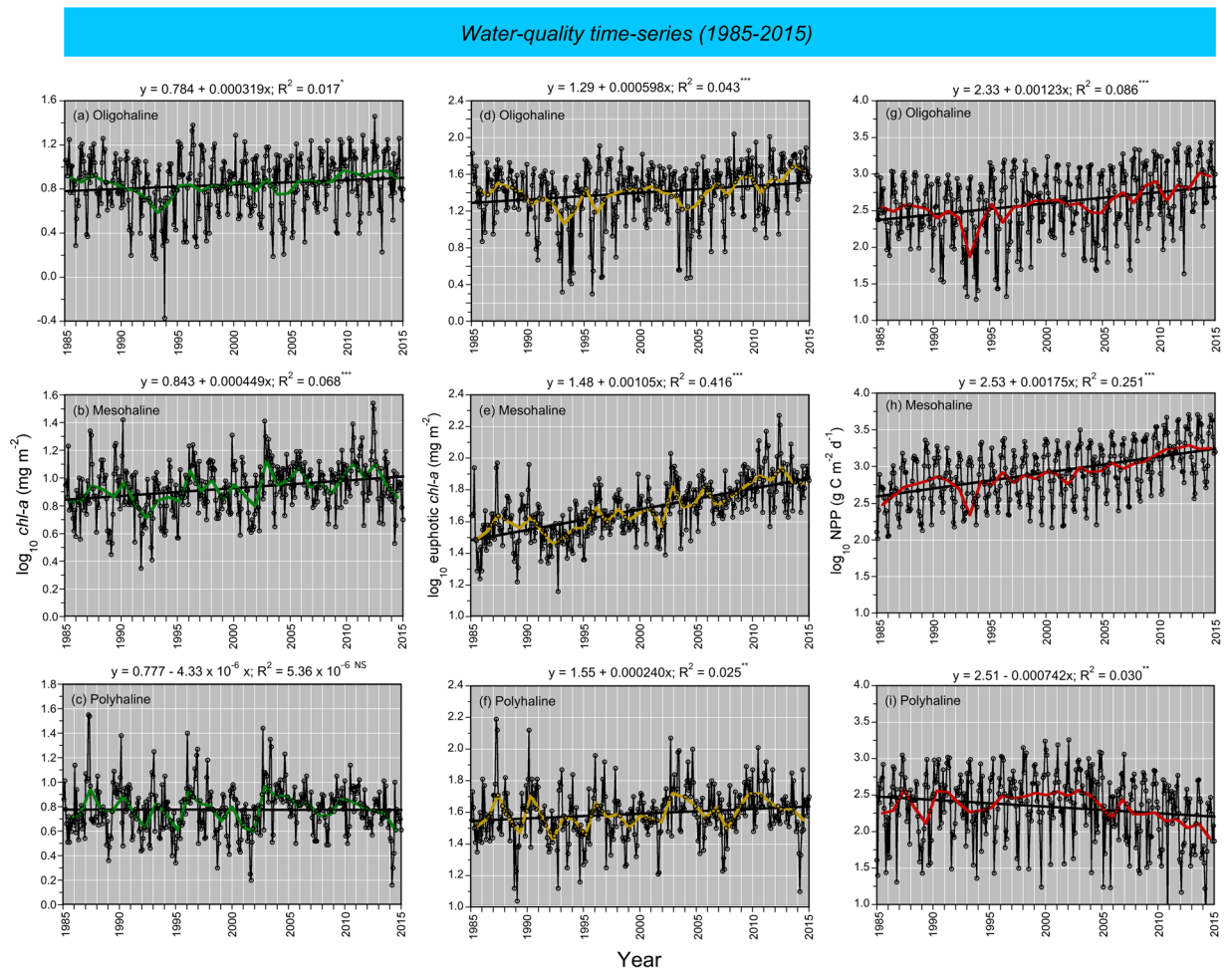


Figure 9. (a–i) Mean, monthly surface $chl-a$ ($mg\ m^{-3}$), euphotic-layer $chl-a$ ($mg\ m^{-2}$) and NPP ($mg\ C\ m^{-2}\ d^{-1}$) for OH, MH, and PH salinity zones from 1985 to 2015. Source data for $chl-a$ and euphotic-layer $chl-a$ were semi-monthly to monthly cruises of the EPA Chesapeake Bay Program (CBP). Model predictions of NPP from gam2 applied to water-quality data from CBP using GAM calibrated with measurements of simulated *in-situ* ^{14}C -bicarbonate assimilation ($n = 713$) and ancillary properties from 1982 to 2004. Climatic effects incorporated using 10th, mean, and 90th percentiles of freshwater flow, salinity, and nutrient (TN, $NO_2 + NO_3$) loading as inputs. Amber dashed lines = low-flow conditions; black solid lines = mean-flow conditions; blue dashed lines = high-flow conditions. Black solid lines = simple, linear regression of model predictions in mean-flow conditions vs time (months), with regression equations superimposed on each panel.

for climatic effects on hydrology (Tables 3, 5; Fig. 10a–f). This approach benefited from the flexibility of GAM to incorporate predictor variables traditionally used in production models, i.e., P_{opt}^B , $chl-a$ or euphotic-layer $chl-a$, Z_p , and SST, and to add variables for salinity zone, salinity, season, SRF, and TN and $NO_2 + NO_3$ loadings.

APPP. Cloern *et al.*⁴ published a synthesis of APPP for estuarine-coastal ecosystems based on a comprehensive survey of the scientific literature. APPP for 131 ecosystems ranged from 105 to 1890 $g\ C\ m^{-2}\ yr^{-1}$, with a mean of 252 $g\ C\ m^{-2}\ yr^{-1}$. Ten-fold variability occurred within ecosystems and five-fold from year to year, with only eight time-series covering longer than a decade. One of the best-studied ecosystems in the survey was the Rhode River, a small sub-estuary adjacent to the MH salinity zone of Chesapeake Bay. Long-term measurements of photosynthesis by Gallegos⁶³ supported estimates of APPP ranging from 152 to 612 $g\ C\ m^{-1}\ yr^{-1}$ in the Rhode River, with a mean of 328 $g\ C\ m^{-1}\ yr^{-1}$. APPP maxima occurred in years with dense spring blooms of *Prorocentrum cordatum* (formerly *P. minimum*) a dinoflagellate species that commonly forms “mahogany tides”. Complex interactions of local and remote nutrient inputs affected the relationship of APPP in the Rhode River to SRF. High-flow conditions displaced the turbidity maximum, usually located in the OH salinity zone, south of the Rhode River mouth, causing elevated turbidity in the sub-estuary, washout of phytoplankton, suppression of the spring bloom, and decreased APPP.

Models of NPP calibrated with long-term measurements in Chesapeake Bay from 1982 to 2004 supported multi-year estimates of APPP, based on water-quality properties from 1985 to 2015 as model inputs. These estimates of APPP allowed us to resolve inter-annual variability for a three-decade span, rarely possible for

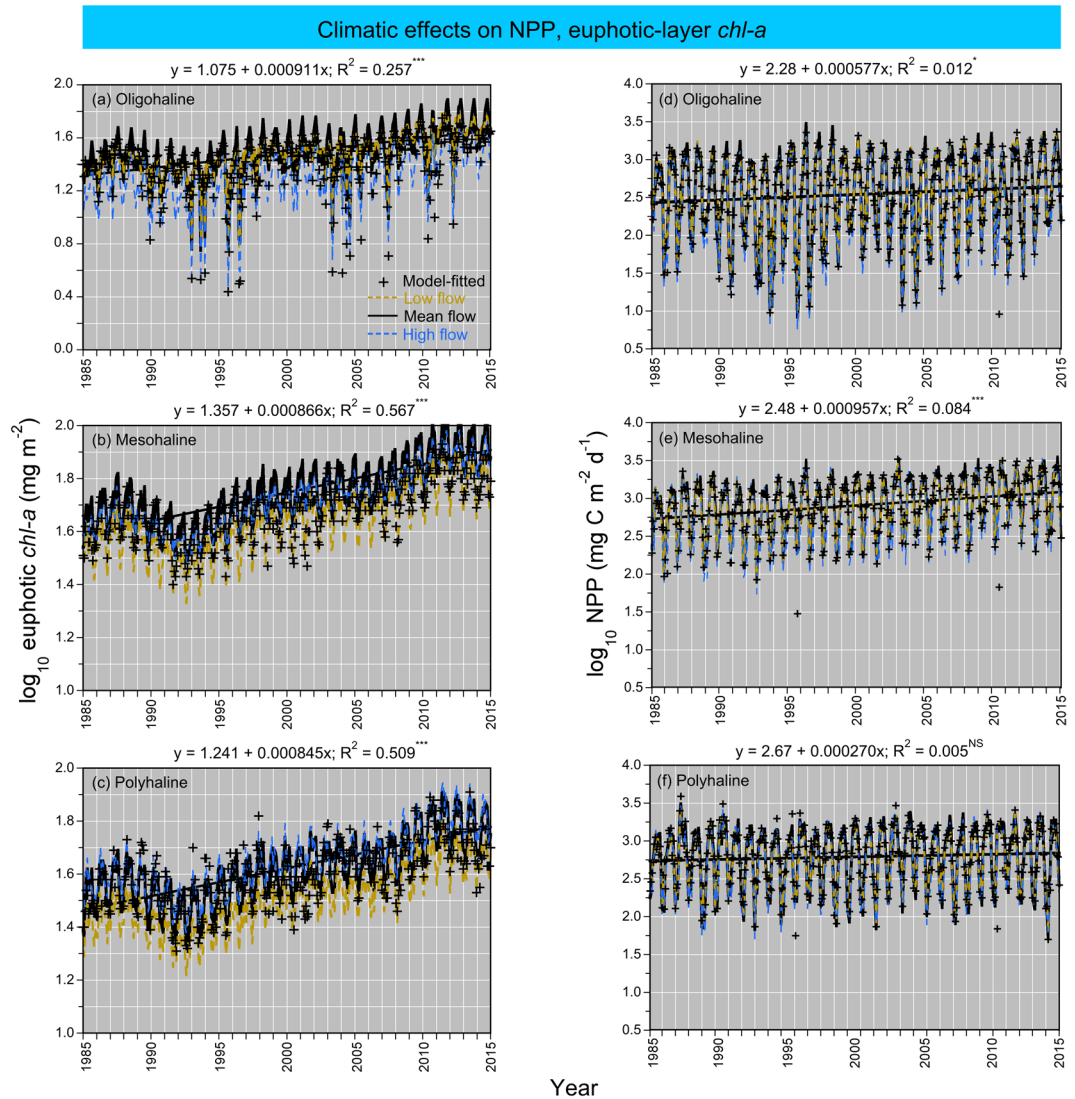


Figure 10. (a–f) Model predictions of \log_{10} euphotic-layer *chl-a* and \log_{10} NPP from 1985 to 2015 using GAM. Flow adjustments were obtained as described in the Fig. 8 caption. Amber dashed lines = low-flow conditions; black solid lines = mean-flow conditions; blue dashed lines = high-flow conditions. Black solid lines = simple, linear regressions of model predictions in mean-flow conditions vs time (months), with equations superimposed on each panel.

estuarine-coastal ecosystems per Cloern *et al.*⁴. Seasonal to inter-annual variability of NPP and thus APPP can be traced to euphotic-layer *chl-a*, a predictor variable that is highly sensitive to climatic effects on hydrology. We previously related inter-annual variability of APPP to TN and TP loadings, based on the supply of new nutrients from the Susquehanna River during the winter–spring freshet⁷. Stepwise regressions tested time lags between the seasonal pulse of nutrients and maximum NPP in summer, identifying mean, monthly TN and TP loads in February and March as predictors of APPP. Models of NPP developed here used a different approach to capture climatic effects on hydrology, explicitly accounting for variability of freshwater flow and nutrient loadings with predictor variables. The resulting model predictions of NPP supported estimates of APPP, resolving inter-annual variability and long-term trends from 1985 to 2015 (Fig. 11a–c).

Nixon’s trophic classification, historical context. Mean-flow predictions of NPP were used to estimate APPP from 130 to >600 g C m⁻² y⁻¹ for OH, MH, and PH salinity zones, with increases from 1985 to 2015 matching euphotic-layer *chl-a* (Fig. 11a–c). APPP of this magnitude corresponds to “eutrophic” for OH and PH salinity zones, and “hypertrophic” for the MH salinity zone using Nixon’s³ trophic classification (Fig. 1). According to Cloern *et al.*⁴, Chesapeake Bay ranks among estuarine-coastal ecosystems that are heavily impacted by nutrient over-enrichment (their Fig. 4). We evaluated prospects for changing trophic classification based on APPP by simulating 40% reductions of biomass or nutrient loadings in models of NPP. These reductions of euphotic-layer *chl-a* or TN and NO₂ + NO₃ loadings led to decreased APPP and changed trophic status from “hypertrophic”

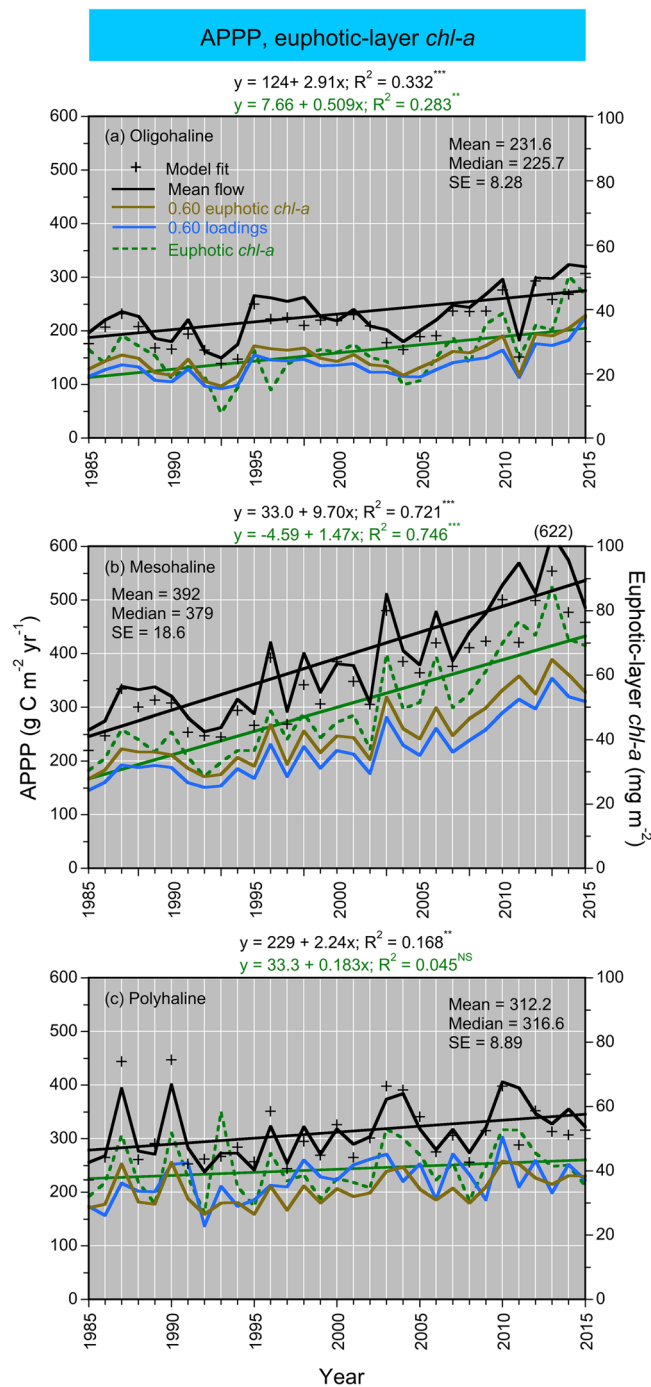


Figure 11. (a–c) Time series of APPP and euphotic-layer *chl-a* from 1985 to 2015 for OH, MH, and PH salinity zones. Crosses = model predictions in ambient conditions; black solid lines = model predictions in mean-flow conditions; amber solid lines = model predictions in mean-flow conditions with 40% reduction of euphotic-layer *chl-a*; blue solid lines = model predictions with 40% reductions of nutrient (TN, $\text{NO}_2 + \text{NO}_3$) loadings; green dashed lines = mean, annual euphotic-layer *chl-a*.

to “eutrophic” for the MH salinity zone, and from “eutrophic” to “mesotrophic” for OH and PH salinity zones (Fig. 11a–c).

Simulated 40% reductions of euphotic-layer *chl-a* or TN and $\text{NO}_2 + \text{NO}_3$ loadings were based on goals established by the 1987 Chesapeake Bay Agreement⁶⁴ to reduce phytoplankton biomass sufficiently to reverse summer anoxia. Several interventions by management began in the 1980s when states bordering the bay banned phosphate in laundry detergents. Subsequent nutrient-management legislation was adopted by Maryland, Virginia, and Pennsylvania in the 1990s, aimed at reducing the over-application of commercial fertilizers and manure on agricultural lands. In 2004, the six states in the watershed, the District of Columbia, and U.S. EPA reached an agreement on comprehensive wastewater treatment permits, leading to numerical annual loading limits for over

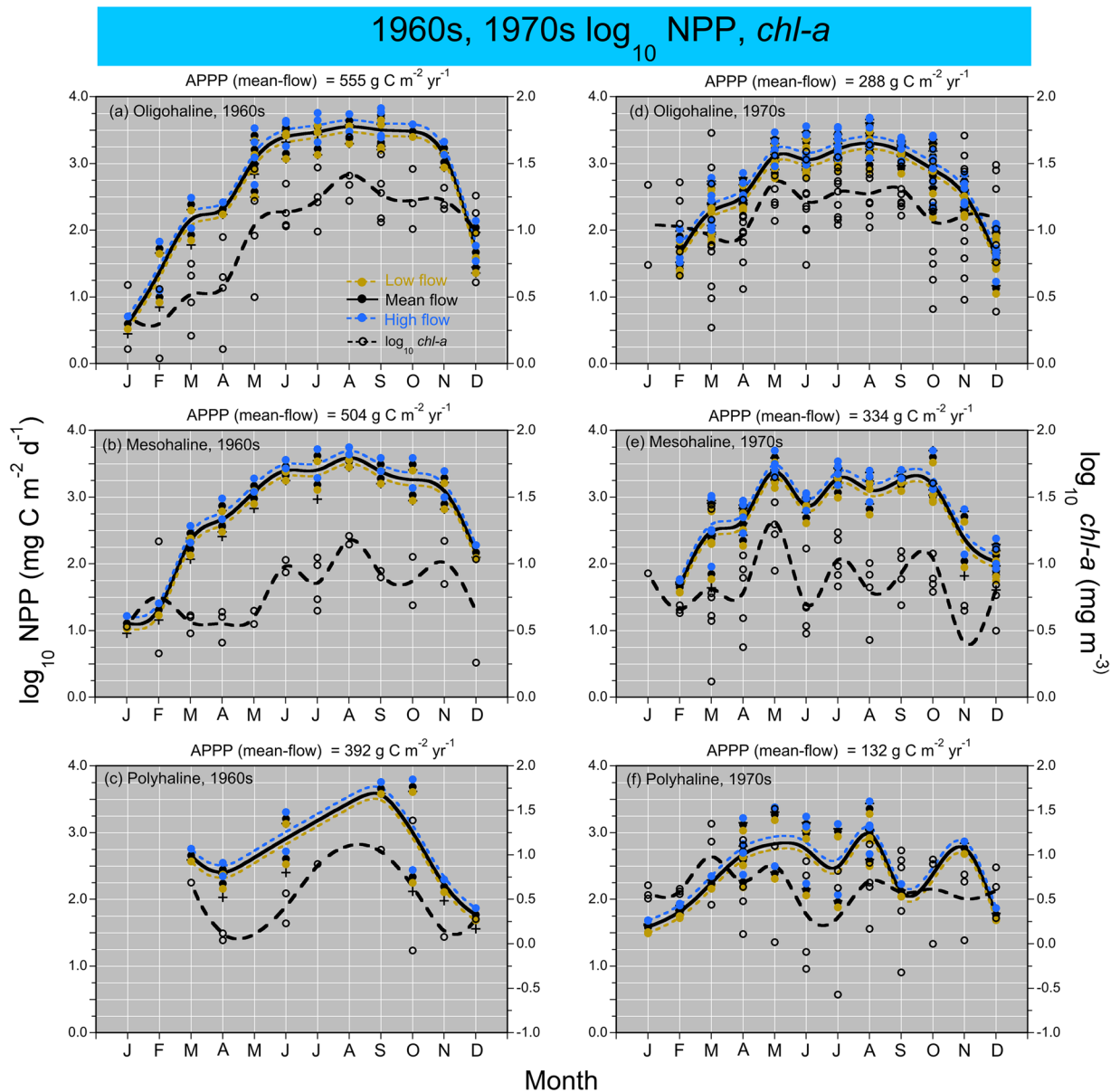


Figure 12. (a–f) Mean, monthly \log_{10} NPP (left y-axis) and \log_{10} *chl-a* (right y-axis) in the 1960s and 1970s for OH, MH, and PH salinity zones. NPP derived using gam5 (Table 4).

470 municipal and industrial wastewater treatment facilities. In December 2010, total manageable daily loads (TMDL) were adopted by U.S. EPA in collaboration with the six states and the District of Columbia. These agreements committed to significant reductions of nutrient and sediment loads by 2025, development of locally based watershed implementation plans, and an accountability system including annual milestones and public reporting of progress.

Together, these actions have led to modest progress toward improved water quality and changes in phytoplankton ecology in the bay¹⁶, although additional nutrient reductions must be reached to decrease APPP and change trophic classification. Our analyses of long-term trends showed flow-adjusted TN and $\text{NO}_2 + \text{NO}_3$ loadings doubled from 1945 to 1981, followed by decreases of 19.2% and 5.3% from 1981 to 2012¹⁶. The slow, upward trajectory of flow-adjusted *chl-a* for the MH salinity zone is consistent with shallow, downward trends of TN and $\text{NO}_2 + \text{NO}_3$ loadings in recent years^{16,18}. We point out that simulated 40% reductions of euphotic-layer *chl-a* or nutrient loadings exceed actual progress since the 1980s, explaining the continuing increases of APPP based on mean-flow model predictions of NPP (Fig. 11a–c).

Decadal contrasts of NPP and APPP in the 1960s and 1970s (Fig. 12a–f) reflected a combination of water-quality management and climatic effects: (1) lower inputs of bio-optically active constituents in the 1960s accompanied a sequence of low-flow, “dry” years compared to the 1970s, reducing light-limitation for OH, MH, and PH salinity zones and enhancing NPP and APPP; (2) removal of orthophosphate (PO_4^{3-}) from detergents enhanced P-limitation in the OH salinity zone, leading to increased N-throughput to MH and PH salinity zones,

Salinity Zone (units)	Season	Z _p (m)	SST (°C)	Salinity	log ₁₀ chl-a (mg m ⁻³)	chl-a	L CI, U CI	log ₁₀ Euc _{chl-a} (mg m ⁻²)	Euc _{chl-a}	L CI, U CI	log ₁₀ NPP (mg C m ⁻² d ⁻¹)	NPP	L CI, U CI	log ₁₀ GPP (mg C m ⁻² d ⁻¹)	GPP	L CI, U CI
OH	Spring	3.45	12.3	3.16	0.764	5.81	(4.57, 7.05)	1.23	17.0	(15.7, 18.3)	2.34	219.9	(218.6, 221.3)	2.51	323.6	(322.2, 325.1)
OH	Summer	4.10	26.4	5.23	0.978	9.50	(8.27, 10.7)	1.56	36.5	(35.2, 37.7)	3.07	1175	(1174, 1176)	3.30	1973	(1971, 1974)
OH	Fall	4.25	16.2	4.65	0.657	4.53	(3.20, 5.87)	1.21	16.0	(14.6, 17.4)	2.47	295.7	(294.3, 297.2)	2.56	363.5	(362.0, 365.0)
MH	Spring	7.15	13.1	11.1	1.13	13.4	(12.2, 14.6)	1.95	88.1	(87.0, 89.3)	2.85	711.7	(710.5, 712.9)	3.07	1180	(1179, 1181)
MH	Summer	6.62	26.7	12.2	1.07	11.8	(10.6, 12.9)	1.85	71.4	(70.3, 72.5)	3.28	1909	(1908, 1910)	3.51	3267	(3266, 3268)
MH	Fall	8.11	18.3	15.0	0.952	8.96	(7.82, 10.1)	1.83	68.1	(66.9, 69.2)	3.02	1056	(1055, 1057)	3.11	1279	(1278, 1280)
PH	Spring	8.74	12.5	19.2	0.823	6.66	(5.40, 7.92)	1.70	49.7	(48.5, 50.9)	2.66	458.9	(457.7, 460.1)	2.85	701.7	(700.5, 702.9)
PH	Summer	9.64	26.4	21.1	0.719	5.24	(4.00, 6.48)	1.58	37.6	(36.5, 38.8)	3.07	1164	(1163, 1165)	3.25	1767	(1765, 1768)
PH	Fall	7.41	18.2	22.8	0.844	6.97	(5.82, 8.13)	1.67	47.1	(45.9, 48.2)	2.90	798.8	(797.8, 799.9)	3.00	1001	(999.8, 1002)

Table 2. Statistical properties of shipboard data from 1982 to 2004 used to calibrate models of net and gross primary production (NPP, GPP). Z_p = euphotic-layer depth, SST = sea-surface temperature; chl-a = chlorophyll a; Euc_{chl-a} = euphotic-layer chl-a; L CI = lower 95% confidence interval; U CI = upper 95% confidence interval.

Predictor variables
log ₁₀ P ^B _{opt} (net or gross)
log ₁₀ euphotic-layer chl-a (or log ₁₀ chl-a)
Salinity zone (categorical)
Sea-surface temperature (SST)
Salinity
K _{PAR} or Z _p (light attenuation coefficient or euphotic-layer depth)
Month (numerical, 1–12)
Season (categorical)
Year (sequential from start of time-series)
log ₁₀ SRF (mean, monthly Susquehanna R. flow)
log ₁₀ SUM (cumulative, monthly Susquehanna R. flow)
TN loading (monthly or annual)
NO ₂ + NO ₃ loading (monthly or annual)

Table 3. Predictor variables for generalized additive models (GAM) of net and gross primary production (NPP, GPP) in Chesapeake Bay.

Property	Time frame	N	R ² (adjusted)	% Deviance explained	GCV	AIC	RMSE
NPP							
OH	1982–2004	183	0.985	98.9	0.00736	−373.1	0.0757
MH		281	0.971	97.6	0.00537	−663.5	0.0661
PH		259	0.955	96.5	0.00807	−478.8	0.0825
GPP							
OH	1995–2004	125	0.961	97.5	0.0217	−141.8	0.1191
MH		210	0.783	82.0	0.0263	−172.4	0.1472
PH		190	0.740	79.5	0.0318	−124.9	0.1575

Table 4. Statistics for generalized additive models (GAM) of net and gross primary production (NPP, GPP) in Chesapeake Bay using predictor variables (Table 3) as detailed for **gam2** (Table 5). GCV = generalized cross-validation score; AIC = Akaike information criterion; RMSE = root mean square error.

and reductions of NPP and APPP from the 1960s to the 1970s; (3) model predictions of NPP for low-flow, “dry”, mean-flow, and high-flow, “wet” conditions were based on predictor variables for flow and salinity that adjusted for climatic effects, with mean-flow predictions of NPP and APPP reflecting these adjustments in the 1960s and 1970s.

Model predictions of NPP from historical reconstructions and recent years led to comparable estimates of APPP for the MH salinity zone. Mean-flow model predictions of NPP produced estimates of APPP > 500 g C m⁻² y⁻¹ from 2010 to 2015 (Fig. 11b), similar to APPP for the same salinity zone in the 1960s (Fig. 12b). Analogous estimates for OH and PH salinity zones showed a similar pattern, with APPP in the 1960s higher than in recent years. APPP was lower for all three salinity zones in the 1970s than in the 1960s (Fig. 12d–f). These observations and predictions provide historical context for comparison with contemporary conditions, suggesting APPP today is not appreciably different from past rates. We found evidence of lower APPP for MH and PH salinity zones in

gam1.pp.net.oh <- gam(log_PP_net ~ s(log_Pbopt_net) + s(log_Euchl) + s(Kpar) + s(Temp) + s(Salin) + s(Month, bs = "cc", k = 8) + s(Seq_year) + Seq_year + Season + s(LOG_SRF) + s(LOG_SUM) + s(TN_LDg) + s(NO23_LDg), data = PP_OH) ^{a,b}
gam2.pp.net.oh <- gam(log_PP_net ~ s(log_Pbopt_net) + s(log_Euchl) + s(Kpar) + s(Temp) + s(Salin) + s(Month, bs = "cc", k = 8) + Season + s(LOG_SRF) + s(LOG_SUM) + s(TN_LDg) + s(NO23_LDg), data = PP_OH) ^c
gam3.pp.net.oh <- gam(log_PP_net ~ s(log_Pbopt_net) + s(log_Ch1) + s(Kpar) + s(Temp) + s(Salin) + s(Month, bs = "cc", k = 8) + Season + s(LOG_SRF) + s(LOG_SUM) + s(TN_LDg) + s(NO23_LDg), data = PP_OH) ^d
gam4.pp.net.oh <- gam(log_PP_net ~ s(log_Pbopt_net) + s(log_Ch1) + s(Temp) + s(Salin) + s(Month, bs = "cc", k = 8) + Season + s(LOG_SRF) + s(LOG_SUM) + s(TN_LDg) + s(NO23_LDg), data = PP_OH) ^e
gam5.pp.net.oh <- gam(log_PP_net ~ s(log_Pbopt_net) + s(log_Ch1) + s(Temp) + s(Salin) + s(Month, bs = "cc", k = 8) + s(LOG_SRF) + s(LOG_SUM) + s(TN_LDg) + s(NO23_LDg), data = PP_OH) ^f

Table 5. GAM models of net primary production (NPP) for the oligohaline (OH) salinity zone. ^agam models of NPP for MH and PH salinity zones had the same structures as these models, using input data PP_MH and PP_PH; models based on the all calibration data (1982 to 2004) used input data PP_ALL and added a categorical term for Salzone (OH, MH, PH); ^bgam models to predict GPP had the same structure as those for NPP with log_Pbopt_gross substituted for log_Pbopt_net; ^bgam2 models applied to water-quality data from 1985 to 2015 were used to predict NPP from data files WQ_OH, WQ_MH, and WQ_PH; the explanatory variable Seq_year was omitted from these models to avoid extending trends in calibration data (1982 to 2004) to years outside that time frame; ^cSubstituted log_Euchl with log_Ch1 in gam models to predict NPP to test models using input data that lacked euphotic-layer *chl-a*; ^dAnnual TN and NO₂ + NO₃ loadings were replaced with monthly loadings in gam models to predict NPP for historical data, based on the lack of data on Kpar or monthly loadings for the 1960s and 1970s; ^eSeason was omitted as a categorical variable in gam models to predict NPP due to small sample sizes for historical data.

Salinity Zone (units)	Season	Z _p (m)	Temp (°C)	Salinity	log ₁₀ <i>chl-a</i> (mg m ⁻³)	<i>chl-a</i>	L CI, U CI	log ₁₀ <i>Euchl-a</i> (mg m ⁻²)	<i>Euchl-a</i>	L CI, U CI	log ₁₀ NPP FIT (mg C m ⁻² d ⁻¹)	NPP FIT	L CI, U CI	log ₁₀ NPP MNS (mg C m ⁻² d ⁻¹)	NPP MNS	L CI, U CI
OH	Winter	4.04	3.73	5.60	0.630	4.30	(3.17, 5.43)	1.21	16.1	(14.9, 17.3)	1.84	69.8	(68.6, 71.0)	1.83	67.4	(66.2, 68.6)
OH	Spring	3.42	11.6	4.76	0.910	8.09	(6.99, 9.19)	1.42	26.4	(25.2, 27.5)	2.53	341.2	(340.0, 342.4)	2.56	361.9	(360.7, 363.1)
OH	Summer	3.54	26.7	6.90	1.09	12.3	(11.3, 13.4)	1.63	42.8	(41.8, 43.9)	3.10	1264	(1263, 1265)	3.09	1239	(1238, 1240)
OH	Fall	4.25	17.3	7.78	0.780	5.99	(4.89, 7.09)	1.39	24.4	(23.3, 25.5)	2.59	386.9	(385.7, 388.2)	2.71	510.6	(509.4, 511.8)
MH	Winter	5.87	11.7	13.6	0.869	7.40	(6.31, 8.49)	1.66	45.7	(44.6, 46.8)	2.47	291.6	(290.4, 292.7)	2.46	290.6	(289.4, 291.7)
MH	Spring	5.39	9.40	12.1	0.957	9.06	(7.94, 10.2)	1.71	50.9	(49.8, 52.0)	2.87	746.3	(745.2, 747.5)	2.91	812.2	(811.1, 813.4)
MH	Summer	5.88	18.2	12.5	1.01	10.2	(9.12, 11.3)	1.70	50.5	(49.4, 51.6)	3.24	1739	(1738, 1740)	3.22	1669	(1668, 1670)
MH	Fall	6.32	18.3	15.5	0.876	7.51	(6.44, 8.58)	1.30	45.9	(44.8, 47.0)	2.93	852.8	(851.7, 853.9)	3.05	1116	(1115, 1117)
PH	Winter	6.89	5.95	20.4	0.740	5.55	(4.55, 6.55)	1.57	36.9	(35.9, 38.0)	2.27	187.6	(186.5, 188.7)	2.21	163.5	(162.4, 164.6)
PH	Spring	7.10	12.2	18.2	0.780	6.03	(5.03, 7.03)	1.62	41.3	(40.2, 42.4)	2.83	672.5	(671.4, 673.7)	2.84	688.8	(687.6, 689.9)
PH	Summer	6.40	26.6	19.8	0.820	6.65	(5.65, 7.65)	1.62	41.8	(40.8, 42.9)	3.17	1489	(1488, 1490)	3.14	1370	(1369, 1371)
PH	Fall	6.71	18.6	21.9	0.770	5.89	(4.83, 6.95)	1.59	38.7	(37.6, 39.7)	2.89	779.7	(778.6, 780.8)	3.09	925.2	(924.1, 926.3)

Table 6. Statistical properties and predicted net primary production (NPP) for water-quality data from 1985 to 2015. NPP FIT = model-fitted NPP using observed flow and salinity; NPP MNS = flow-adjusted NPP using long-term means of freshwater flow and salinity.

contemporary estimates, and sensitivity of APPP to reductions of euphotic-layer *chl-a* or TN and NO₂ + NO₃ loadings. These findings show promise for future reductions of APPP in response to improvements of water quality that would be required to change trophic classification.

Summary

Statistical models of NPP and GPP were developed for Chesapeake Bay with adjustments for climatic effects on hydrology, calibrated with 100 s of shipboard measurements from 1982 to 2004. Model predictions of NPP based on water-quality properties in the 1960s and 1970s and 1985 to 2015 as inputs supported computations of APPP. Simulated reductions of euphotic-layer *chl-a* or TN and NO₂ + NO₃ loadings led to decreased APPP sufficient to change the trophic classification of the bay. Summarizing:

- Statistical models of NPP and GPP calibrated with long-term data included explicit terms to adjust for climatic effects.
- These models supported predictions of NPP using historical and monitoring data as predictor variables.
- Model predictions of NPP using historical (1960s, 1970s) and monitoring (1985 to 2015) data as predictor variables supported computations of APPP.
- Simulated 40% decreases of euphotic-layer *chl-a* or TN and NO₂ + NO₃ loadings reduced APPP and changed trophic classification.
- Improved water quality is attainable with a reversal of nutrient over-enrichment of the bay sufficient to decrease phytoplankton biomass, but progress to date has been modest compared to goals, exemplified by continuing, high APPP in recent years.

Received: 3 November 2019; Accepted: 20 January 2020;

Published online: 06 February 2020

References

- Chavez, F. P., Messié, M. & Pennington, J. T. Marine primary production in relation to climate variability and climate change. *Ann. Rev. Mar. Sci.* **3**, 227–260 (2011).
- Cloern, J. E. Our evolving conceptual model of the coastal eutrophication problem. *Mar. Ecol. Prog. Ser.* **210**, 223–253 (2001).
- Nixon, S. W. Coastal marine eutrophication: a definition, social causes, and future concerns. *Ophelia* **41**, 199–219 (1995).
- Cloern, J. E., Foster, S. Q. & Kleckner, A. E. Phytoplankton primary production in the world's estuarine-coastal ecosystems. *Biogeosci.* <https://doi.org/10.5194/bg-11-2477-2014> (2014).
- Cloern, J. E. & Jassby, A. D. Drivers of change in estuarine systems: discoveries from four decades of study in San Francisco Bay. *Rev. Geophys.* **50**, RG4001, 2–33 (2012).
- Cloern, J. E. & Jassby, A. D. Patterns and scales of phytoplankton variability in estuarine-coastal ecosystems. *Estuar. Coasts* **33**, 230–241 (2010).
- Harding, L. W., Jr., Mallonee, M. E. & Perry, E. S. Toward a predictive understanding of primary productivity in a temperate, partially stratified estuary. *Estuar. Coast. Shelf Sci.* **55**, 437–463 (2002).
- Behrenfeld, M. J. & Falkowski, P. G. Photosynthetic rates derived from satellite-based chlorophyll concentrations. *Limnol. Oceanogr.* **42**, 1–20 (1997).
- Flemer, D. A. Primary production in the Chesapeake Bay. *Chesapeake Sci.* **11**, 117–129 (1970).
- Harding, L. W., Jr., Meeson, B. W. & Fisher, T. R. Photosynthesis patterns in Chesapeake Bay phytoplankton: short- and long-term responses of P-I curve parameters to light. *Mar. Ecol. Prog. Ser.* **26**, 99–111 (1985).
- Harding, L. W., Jr., Meeson, B. W. & Fisher, T. R. Phytoplankton production in two East coast estuaries: photosynthesis-light functions and patterns of carbon assimilation in Chesapeake and Delaware Bays. *Estuar. Coast. Shelf Sci.* **23**, 773–806 (1986).
- Malone, T. C. *et al.* Lateral variation in the production and fate of phytoplankton in a partially stratified estuary. *Mar. Ecol. Prog. Ser.* **32**, 149–160 (1986).
- Malone, T. C., Crocker, L. H., Pike, S. E. & Wendler, B. W. Influence of river flow on the dynamics of phytoplankton in a partially stratified estuary. *Mar. Ecol. Prog. Ser.* **48**, 235–249 (1988).
- Malone T. C. Effects of water column processes on dissolved oxygen: nutrients, phytoplankton and zooplankton. In: Smith, D., Leffler, M., Mackiernan, G. (Eds.), *Oxygen dynamics in Chesapeake Bay: A synthesis of research*, pp. 61–112, University of Maryland Sea Grant, College Park, Maryland, USA (1992).
- Kemp, W. M., Smith, E. M., Marvin-DiPasquale, M. & Boynton, W. R. Organic carbon balance and net ecosystem metabolism in Chesapeake Bay. *Marine Ecology Progress Series* **150**, 229–248 (1997).
- Harding, L. W., Jr. *et al.* Long-term trends of nutrients and phytoplankton in Chesapeake Bay. *Estuar. Coasts* **39**, 664–681 (2016a).
- Harding, L. W., Jr. *et al.* Variable climatic conditions dominate recent phytoplankton dynamics in Chesapeake Bay. *Sci. Rep.* **6**, No. 23773, <https://doi.org/10.1038/srep23773> (2016b).
- Harding, L. W., Jr. *et al.* Long-term trends, current status, and transitions of water quality in Chesapeake Bay. *Sci. Rep.* **9**, Art. No. 6709 (2019).
- Harding, L. W., Jr. *et al.* Climate effects on phytoplankton floral composition in Chesapeake Bay. *Estuar. Coast. Shelf Sci.* **162**, 53–68 (2015).
- Harding, L. W., Jr. Long-term trends in the distribution of phytoplankton in Chesapeake Bay: roles of light, nutrients and streamflow. *Mar. Ecol. Prog. Ser.* **104**, 267–291 (1994).
- Harding, L. W., Jr. & Perry, E. S. Long-term increase of phytoplankton biomass in Chesapeake Bay, 1950–94. *Mar. Ecol. Prog. Ser.* **157**, 39–52 (1997).
- Malone, T. C., Conley, D. J., Fisher, T. R., Glibert, P. M. & Harding, L. W., Jr. Scales of nutrient limited phytoplankton productivity in Chesapeake Bay. *Estuaries* **19**, 371–385 (1996).
- Harding, L. W., Jr., Degobbi, D. & Precali, R. Production and fate of phytoplankton: annual cycles and interannual variability. In: *Ecosystems at the Land-Sea Margin: Drainage Basin to Coastal Sea* (Malone, T.C. *et al.* eds) (1999).
- Fisher, T. R., Harding, L. W., Stanley, D. W. & Ward, L. G. Phytoplankton, nutrients and turbidity in the Chesapeake, Delaware and Hudson estuaries. *Estuar. Coast. Shelf Sci.* **27**, 61–93 (1988).
- Fisher, T. R., Peele, E. R., Ammerman, J. W. & Harding, L. W., Jr. Nutrient limitation of phytoplankton in Chesapeake Bay. *Mar. Ecol. Prog. Ser.* **82**, 51–63 (1992).
- Kemp, W. M. & Boynton, W. R. Spatial and temporal coupling of nutrient inputs to estuarine production: the role of particulate transport and decomposition. *Bull. Mar. Sci.* **3**, 242–247 (1984).
- McCarthy, J. J., Taylor, W. R. & Loftus, M. E. Significance of nanoplankton in the Chesapeake Bay estuary and problems associated with the measurement of nanoplankton productivity. *Mar. Biol.* **24**, 7–16 (1974).
- Malone, T. C., Ducklow, H. W., Peele, E. F. & Pike, S. E. Picoplankton carbon flux in Chesapeake Bay. *Mar. Ecol. Prog. Ser.* **78**, 11–22 (1991).
- Boynton, W. R., Garber, J. H., Summers, R. & Kemp, W. M. Inputs, transformations, and transport of nitrogen and phosphorus in Chesapeake Bay and selected tributaries. *Estuaries* **18**, 285–314 (1995).
- Hagy, J. D. III, Boynton, W. R., Wood, C. W. & Wood, K. V. Hypoxia in Chesapeake Bay, 1950–2001: Long-term change in relation to nutrient loading and river flow. *Estuar. Coasts* **27**, 634–658 (2004).
- Son, S., Wang, M. & Harding, L. W., Jr. Satellite-measured net primary production in the Chesapeake Bay. *Remote Sens. Environ.* **144**, 109–119, <https://doi.org/10.1016/j.rse.2014.01.018> (2014).
- Gallegos, C. L., Werdell, P. J. & McClain, C. R. Long-term changes in light scattering in Chesapeake Bay inferred from Secchi depth, light attenuation, and remote sensing measurements. *J. Geophys. Res. (Oceans)* **116**, C00H08, <https://doi.org/10.1029/2011JC007160> (2011).
- U.S. Environmental Protection Agency, 2003. *Ambient water quality criteria for dissolved oxygen, water clarity and chlorophyll a for Chesapeake Bay and its tidal tributaries*. EPA 903-R-03-002. U.S. Environmental Protection Agency, Region 3, Chesapeake Bay Program Office, Annapolis, Maryland, USA (2003).
- U.S. Environmental Protection Agency, 2012. *Guide to using Chesapeake Bay Program water quality monitoring data*. U.S. Environmental Protection Agency, Region 3, Chesapeake Bay Program Office, Annapolis, Maryland, USA. EPA 903-R-12-001, CBP/TRS 304–12, 155 p. (2012)
- D'Elia, C. F. *et al.* Nitrogen and phosphorus determinations in estuarine waters: a comparison of methods used in Chesapeake Bay Monitoring. CBP/TRS 7/87, Chesapeake Bay Program Office, Annapolis, Maryland (1987).
- Wood, S. N. Stable and efficient multiple smoothing parameter estimation for generalized additive models. *J. Amer. Stat. Assoc.* **99**, 673–686 (2004).
- Wood, S. N. *Generalized additive models (An introduction with R)*. Chapman & Hall/CRC, Boca Raton, Florida, 392 p. (2006).
- Wood, S. N. Low rank scale invariant tensor product smooths for generalized additive mixed models. *Biometrics* **62**, 1025–1036 (2006).

39. Beck, M. W. & Murphy, R. R. Numerical and qualitative contrasts of two statistical models for water quality change in tidal waters. *J. Amer. Water Res. Assoc.* **53**, <https://doi.org/10.1111/1752-1688.12489> (2016).
40. Hirsch, R. M., Moyer, D. L. & Archfield, S. A. Weighted regressions on time, discharge, and season (WRTDS), with an application to Chesapeake Bay river inputs. *J. Amer. Water Res. Assoc.* **45**, 857–880 (2010).
41. Ryther, J. H. & Yentsch. The estimation of phytoplankton production in the ocean from chlorophyll and light data. *Limnol. Oceanogr.* **2**, 281–286 (1957).
42. Talling, J. F. The phytoplankton population as a compound photosynthetic system. *New Phytologist* **56**, 133–149 (1957).
43. Bannister, T. T. Production equations in terms of chlorophyll concentration, quantum yield, and upper limit to production. *Limnol. Oceanogr.* **19**, 1–12 (1974).
44. Smith, R. C. & Baker, K. S. The bio-optical state of ocean waters and remote sensing. *Limnol. Oceanogr.* **23**, 247–259 (1978).
45. Lewis, M., Warnock, R. E. & Platt, T. Photosynthetic response of marine picoplankton at low photon flux. In: *Photosynthetic Picoplankton. Canada Bull. Fish. Aquat. Sci.* **214**, 235–250 (1987).
46. Banse, K. & Yong, M. Sources of variability in satellite-derived estimates of phytoplankton production in the eastern tropical Pacific. *J. Geophys. Res.* **95**(7), 201–7,215 (1990).
47. Balch, W. M. & Byrne, C. F. Factors affecting the estimation of primary production from space. *J. Geophys. Res.* **99**(7), 555–7,570 (1994).
48. Cole, B. E. & Cloern, J. E. Significance of biomass and light availability to phytoplankton productivity in San Francisco Bay. *Mar. Ecol. Prog. Ser.* **17**, 15–24 (1984).
49. Cole, B. E. & Cloern, J. E. An empirical model for estimating phytoplankton primary productivity in estuaries. *Mar. Ecol. Prog. Ser.* **36**, 299–305 (1987).
50. Campbell, J. W. & O'Reilly, J. E. Role of satellites in estimating primary productivity from space. *Cont. Shelf Res.* **8**, 179–204 (1988).
51. Cloern, J. E. *et al.* River discharge controls phytoplankton dynamics in the northern San Francisco Bay estuary. *Estuar. Coast. Shelf Sci.* **16**, 415–429 (1983).
52. Mallin, M. A., Paerl, H. W., Rudek, J. & Bates, P. W. Regulation of estuarine primary production by watershed rainfall and river flow. *Mar. Ecol. Prog. Ser.* **93**, 199–203 (1993).
53. Miller, W. D. Climate forcing of phytoplankton dynamics in Chesapeake Bay. Ph.D. Dissertation, University of Maryland, College Park, Maryland, 168 p. (2006).
54. Adolf, J. E., Yeager, C. L., Miller, W. D., Mallonee, M. E. & Harding, L. W., Jr. Environmental forcing of phytoplankton floral composition, biomass, and primary productivity in Chesapeake Bay, USA. *Estuar. Coast. Shelf Sci.* **67**, 108–122 (2006).
55. Boynton, W. R. & Kemp, W. M. Influence of river flow and nutrient loads on selected ecosystem processes: A synthesis of Chesapeake Bay data. In *Estuarine science, a synthetic approach to research and practice*, ed. Hobbie, J. E. 269–298. Washington, D.C.: Island Press (2000).
56. Howarth, R. W., Swaney, D., Butler, T. J. & Marino, R. Climatic control on eutrophication of the Hudson River estuary. *Ecosystems* **3**, 210–215 (2000).
57. Acker, J. G., Harding, L. W., Leptoukh, G., Zhu, T. & Shen, S. Remotely-sensed chl *a* at the Chesapeake Bay mouth is correlated with annual freshwater flow to Chesapeake Bay. *Geophys. Res. Lett.* **32**, L05601 (2005).
58. Paerl, H. W., Valdes, L. M., Peierls, B. L., Adolf, J. E. & Harding, L. W., Jr. Anthropogenic and climatic influences on the eutrophication of large estuarine ecosystems. *Limnol. Oceanogr.* **51**, 448–462 (2006).
59. Paerl, H. W., Hall, N. S., Peierls, B. L., Rossignol, K. L. & Joyner, A. R. Hydrologic variability and its control of phytoplankton community structure and function in two shallow, coastal, lagoonal ecosystems: the Neuse and New River estuaries, North Carolina, USA. *Estuar. Coasts* <https://doi.org/10.1007/s12237-013-9686-0> (2013).
60. Miller, W. D. & Harding, L. W., Jr. Climate forcing of the spring bloom in Chesapeake Bay. *Mar. Ecol. Prog. Ser.* **331**, 11–22 (2007).
61. Miller, W. D., Kimmel, D. G. & Harding, L. W., Jr. Predicting spring discharge of the Susquehanna River from a winter synoptic climatology for the eastern United States. *Water Resources Res.* **42**, W05414, <https://doi.org/10.1029/2005WR004270> (2006).
62. Kimmel, D. G., Miller, W. D., Harding, L. W., Jr., Houde, E. D. & Roman, M. R. Estuarine ecosystem response captured using a synoptic climatology. *Estuar. Coasts* **32**, 403–409 (2009).
63. Gallegos, C. L. Long-term variations in primary production in a eutrophic sub-estuary. II Interannual variations and modeling. *Mar. Ecol. Prog. Ser.* **502**, 69–83 (2014).
64. Chesapeake Bay Agreement. Chesapeake Bay Executive Committee, 15 December 1987, Annapolis, Maryland, 7 pp (1987).

Acknowledgements

We thank Bill Boicourt, Walt Boynton, D. Wayne Coats, Tom Fisher, Kelly Henderson, Ed Houde, Christy Jordan, Mike Kemp, Mike Lomas, Andrea Magnuson, Tom Malone, Blanche Meeson, Sherry Pike, Mike Roman, Michele Scardi, Erik Smith, Bess Ward, and the captains and crews of the research vessels *Aquarius*, *Cape Hatteras*, *Cape Henlopen*, and *Ridgely Warfield*, and for contributions to this work. Support from multiple awards by the National Science Foundation (NSF), National Aeronautics and Space Administration (NASA), Maryland Sea Grant, and U.S. Environmental Protection Agency (EPA) over a period of >30 years is gratefully acknowledged.

Author contributions

L.W.H., M.E.M., E.S.P., W.D.M., J.E.A., C.L.G. and H.W.P. contributed to data analysis and manuscript preparation. L.W.H. and E.S.P. conducted statistical analyses. L.W.H. and C.L.G. prepared the figures. L.W.H. wrote the main text of the manuscript.

Competing interests

The authors declare no competing interests.

Additional information

Correspondence and requests for materials should be addressed to L.W.H.

Reprints and permissions information is available at www.nature.com/reprints.

Publisher's note Springer Nature remains neutral with regard to jurisdictional claims in published maps and institutional affiliations.



Open Access This article is licensed under a Creative Commons Attribution 4.0 International License, which permits use, sharing, adaptation, distribution and reproduction in any medium or format, as long as you give appropriate credit to the original author(s) and the source, provide a link to the Creative Commons license, and indicate if changes were made. The images or other third party material in this article are included in the article's Creative Commons license, unless indicated otherwise in a credit line to the material. If material is not included in the article's Creative Commons license and your intended use is not permitted by statutory regulation or exceeds the permitted use, you will need to obtain permission directly from the copyright holder. To view a copy of this license, visit <http://creativecommons.org/licenses/by/4.0/>.

© The Author(s) 2020